EVALUATING FRP REPAIR METHOD FOR CRACKED PRESTRESSED CONCRETE BRIDGE MEMBERS SUBJECTED TO REPEATED LOADINGS PHASE 1

Calvin E. Reed
Kansas Department of Transportation
Topeka, Kansas

Robert J. Peterman
Hayder A. Rasheed
Kansas State University
Manhattan, Kansas

APRIL 2005

K-TRAN

A COOPERATIVE TRANSPORTATION RESEARCH PROGRAM BETWEEN:
KANSAS DEPARTMENT OF TRANSPORTATION
KANSAS STATE UNIVERSITY
THE UNIVERSITY OF KANSAS

1 Report No. K-TRAN: KSU-01-2	2 Government Accession No.	3 Recipient Catalog No.
4 Title and Subtitle EVALUATING FRP REPAIR METHOD FOR CRACKED PRESTRESSED CONCRETE BRIDGE MEMBERS SUBJECTED TO REPEATED LOADINGS (PHASE 1)		**5 Report Date** April 2005
		6 Performing Organization Code
7 Author(s) Calvin E. Reed*, Kansas Department of Transportation; Robert J. Peterman and Hayder A. Rasheed, Kansas State University *Affiliation at time of research report, current affiliation not known.		**8 Performing Organization Report No.**
9 Performing Organization Name and Address Kansas State University; Department of Civil Engineering 2118 Fiedler Hall Manhattan, Kansas 66506		**10 Work Unit No. (TRAIS)**
		11 Contract or Grant No. C1245
12 Sponsoring Agency Name and Address Kansas Department of Transportation Bureau of Materials and Research 700 SW Harrison Street Topeka, Kansas 66603-3754		**13 Type of Report and Period Covered** Final Report March 2001 – April 2004
		14 Sponsoring Agency Code RE-0233-01

15 Supplementary Notes
For more information write to address in block 9.

16 Abstract

This report presents the details of a research study on the use of carbon fiber reinforced polymer (CFRP) sheets to repair and strengthen prestressed concrete bridge girders in flexure and shear. Five specimens that were removed from an overloaded bridge (Bridge #56) in Graham County, Kansas were tested. Three of the beams were statically tested to failure to determine their flexural capacity with and without strengthening. It was found that longitudinal CFRP sheets significantly increased the ultimate flexural capacity of the specimens. The other two specimens were tested in fatigue. High stress ranges in the prestressing strands caused the early failure of both specimens. Failure of Specimen 4 occurred by rupture of strands at the location of the mid-span push down device. A special strengthening scheme was applied to Specimen 5 to reduce any tensile stress concentration expected to develop at the push down device detail of the harped strands. This scheme successfully protected the push down device area causing failure to shift outside the mid span region, where higher strand stress range existed. Corrosion may have also contributed to the premature failure. Shear capacity was also examined on the two ends of each of the failed specimens. Two cases were evaluated in shear. The first one had the applied load such that shear cracks would form within the transfer length of the prestressing strands (allowing a bond-slip failure within that region). The second case had the applied load outside the transfer length of the prestressing strand (preventing bond-slip failure). The test results showed that transverse CFRP sheets increased the shear capacity of the specimens tested, but did not prevent bond-slip failures when diagonal cracks propagated into the transfer zone.

17 Key Words Bridge Girders, Carbon Fiber Reinforced Polymer, CFRP, Cracking, Fatigue and Prestressed Concrete	**18 Distribution Statement** No restrictions. This document is available to the public through the National Technical Information Service, Springfield, Virginia 22161	
19 Security Classification (of this report) Unclassified	**20 Security Classification (of this page)** Unclassified	**21 No. of pages** 117	**22 Price**

Form DOT F 1700.7 (8-72)

EVALUATING FRP REPAIR METHOD FOR CRACKED PRESTRESSED CONCRETE BRIDGE MEMBERS SUBJECTED TO REPEATED LOADINGS (PHASE 1)

Final Report

Prepared by

Calvin E. Reed*
Kansas Department of Transportation

Robert J. Peterman
Kansas State University

And

Hayder A. Rasheed
Kansas State University

*Affiliation at time of research report, current affiliation not known.

PREFACE

The Kansas Department of Transportation's (KDOT) Kansas Transportation Research and New-Developments (K-TRAN) Research Program funded this research project. It is an ongoing, cooperative and comprehensive research program addressing transportation needs of the state of Kansas utilizing academic and research resources from KDOT, Kansas State University and the University of Kansas. Transportation professionals in KDOT and the universities jointly develop the projects included in the research program.

NOTICE

The authors and the state of Kansas do not endorse products or manufacturers. Trade and manufacturers names appear herein solely because they are considered essential to the object of this report.

This information is available in alternative accessible formats. To obtain an alternative format, contact the Office of Transportation Information, Kansas Department of Transportation, 700 SW Harrison, Topeka, Kansas 66603-3754 or phone (785) 296-3585 (Voice) (TDD).

DISCLAIMER

The contents of this report reflect the views of the authors who are responsible for the facts and accuracy of the data presented herein. The contents do not necessarily reflect the views or the policies of the state of Kansas. This report does not constitute a standard, specification or regulation.

ABSTRACT

This report presents the details of a research study on the use of carbon fiber reinforced polymer (CFRP) sheets to repair and strengthen prestressed concrete bridge girders in flexure and shear. Five specimens that were removed from an overloaded bridge (Bridge #56) in Graham County, Kansas were tested. Three of the beams were statically tested to failure to determine their flexural capacity with and without strengthening. It was found that longitudinal CFRP sheets significantly increased the ultimate flexural capacity of the specimens. The other two specimens were tested in fatigue. High stress ranges in the prestressing strands caused the early failure of both specimens. Failure of Specimen 4 occurred by rupture of strands at the location of the mid-span push down device. A special strengthening scheme was applied to Specimen 5 to reduce any tensile stress concentration expected to develop at the push down device detail of the harped strands. This scheme successfully protected the push down device area causing failure to shift outside the mid span region, where higher strand stress range existed. Corrosion may have also contributed to the premature failure. Shear capacity was also examined on the two ends of each of the failed specimens. Two cases were evaluated in shear. The first one had the applied load such that shear cracks would form within the transfer length of the prestressing strands (allowing a bond-slip failure within that region). The second case had the applied load outside the transfer length of the prestressing strand (preventing bond-slip failure). The test results showed that transverse CFRP sheets increased the shear capacity of the specimens tested, but did not prevent bond-slip failures when diagonal cracks propagated into the transfer zone.

ACKNOWLEDGEMENTS

TABLE OF CONTENTS

LIST OF FIGURES

LIST OF TABLES

Chapter 1

Introduction

1.1   Background

The bridge and highway infrastructure in the United States is aging. According to the Federal

Highway Administration (FHWA), nearly 61% of the over 584,000 bridges in the United States

were built prior to 1970 (FHWA 2001). Many of these older bridges have been loaded to levels

that are beyond the service limits the bridges were initially designed for. When this occurs,

damage to the structure is typically the result. Repair and strengthening of bridges is becoming

an attractive way of extending the useful life of a bridge. For a strengthening technique to be

beneficial, however, it must be able to reliably strengthen the structure for a long period of time

and be cost effective.

Techniques for repairing and strengthening reinforced and prestressed concrete bridge

girders have been widely investigated over the past twenty years. Much research has gone into

increasing the flexural and shear capacity of these members by means of externally bonded

reinforcement. Initially, steel plates were bonded to the concrete members in the tensile zones to

provide flexural reinforcement (Dussek 1980). However, corrosion of the steel was a problem

under normal environmental conditions and led researchers to search out a more environmentally

inert material for reinforcement. More recently, the use of Fiber Reinforced Polymers (FRP) has

been widely investigated because of their ability to withstand corrosion under normal

environmental conditions in addition to their high strength and stiffness to weight ratios, ease of

installation and potentially low maintenance cost.

FRP is the general name for a class of composite materials in which fibers (generally

Glass, Carbon, or Aramid) are suspended in a cured polymer matrix. They have been used

extensively in the aerospace and automobile industries for many years and have just recently begun to make their way into civil infrastructure applications. The material comes in different shapes and sizes including bars (similar to steel rebar), woven sheets with fibers running in one or two directions (unidirectional and bi-directional, respectively), and pre-cured plates. The mechanical properties generally show the same trend of linear-elastic response to failure and relatively high Young's modulus (E) and ultimate strength, when the loading is aligned with the fiber direction.

Fanning and Kelly (2001) have shown that as much as 40% increase in flexural stiffness and a 70% increase in ultimate strength of RC beams can be accomplished with CFRP plates. Others reported a wider spectrum of increase in ultimate strength ranging from 20% (Norris et al. 1997) to 275% (Quantrill et al. 1996). Research by Arduini and Nanni (1997) has also shown that CFRP sheets, when applied to pre-cracked RC members, can significantly improve the ultimate flexural capacity as well as increase flexural stiffness. It has also been shown that application of CFRP plates to full-scale structures is relatively easy and provides an increase in flexural capacity (Nanni 1995 and Alkhradaji et al. 2000).

1.2   CFRP: Applications in Kansas

According to the FHWA, nearly 26% of the over 25,700 bridges in Kansas are labeled either structurally deficient or functionally obsolete (compared to 29% national average). Of these, over 2,100 are reinforced or prestressed concrete bridges (FHWA, 2001). Many of these bridges were designed in the 1960's and 1970's to carry AASHTO H-15 design live load on rural county roads. In many cases, frequent overloading has occurred due to the heavier vehicles now traveling on these structures. This has led to significant cracking of the concrete members and in some cases spalling of concrete. Because cracked prestressed members are especially susceptible

to strand fatigue as well as corrosion, the damaged girders on these bridges need to be repaired or replaced.

One such bridge in which multiple overloads had occurred is Bridge #56 in Graham County, Kansas (located about 5 km (3 miles) south of Penokee). The four-span bridge was composed of prestressed double-tee members. In the late 1990's, inspection of the bridge showed that most of the stems of the interior double-tees were severely cracked and in some cases spalling had occurred. Consequently, the damaged girders were removed and replaced.

Upon removal, three of the girders were sent to Newton, Kansas, where they were saw cut longitudinally providing six single-tee test specimens. Five of the specimens were shipped to Kansas State University for experimental testing. The testing involved application of various levels of Carbon FRP sheets for flexural and shear strengthening. The beams were then tested to failure at the Civil Infrastructure Systems Laboratory (CISL). Results and conclusions from these tests are reported in the following chapters.

Chapter 2

Objectives

This experimental and analytical study had three primary objectives. The first objective of this study was to evaluate the flexural behavior of prestressed concrete beams strengthened with CFRP laminates. Static tests to failure were run on three of the specimens to determine the effect of strengthening on the improvement of strength and stiffness. Fatigue tests were run on two of the specimens to determine the degradation of strength and stiffness under repeated load cycles.

The second objective of this study was to evaluate the shear behavior of the specimens. Static tests to failure were performed on both ends of each specimen. In one test setup, shear cracks were allowed to develop near the girder end, within the prestress force transfer zone causing a bond-slip failure to occur. In the other setup, the shear cracks were allowed to develop away from the prestress transfer zone causing a shear failure to occur. The ability of the CFRP to strengthen the specimens against both failure modes was examined.

The third objective of this study was to develop an analytical model to predict the flexural behavior of the specimens (Chapter 5). The analytical results were correlated with experimental results to determine model accuracy. An accurate model will prove useful for KDOT in future design and analysis of FRP strengthened prestressed and reinforced concrete beams.

Chapter 3

Literature Review

This chapter will highlight the research studies in the literature that were reviewed for the purpose of this report. The papers will be presented chronologically according to their publishing date with the earlier articles coming first. Full citation for these articles can be found in the references section of the report.

The earliest experimental studies undertaken in the United States, on strengthened beams, was conducted at the University of Arizona at Tucson (Saadatamanesh and Ehsani 1990-1991). In the first series (Saadatamanesh and Ehsani 1990), four RC beams (90 mm by 150 mm by 1675 mm) were externally strengthened with epoxy bonded Glass fiber reinforced sheets (6mm thick and 75mm wide) for the full length of the test specimens. All four beams and the control specimen were reinforced with one 9.5mm reinforcing bar. The shear reinforcement consisted of 5mm diameter wires spaced at 75 mm. All beams were simply supported and subjected to four-point bending. Four different epoxy adhesive systems were investigated. The first one had a rubbery texture with tensile lap shear strength of 13MPa. In this specimen, the stiffness started to decrease sharply once the beam began to crack. Failure was ductile with minor plate separation, which was due to the high flexibility of the epoxy that allowed for little shear transfer. A tougher two-component epoxy with tensile lap shear strength of 14 MPa was used in the second beam and the results showed a larger increase in the overall stiffness of the beam. Failure was attributed to shear cracks resulting in plate separation and a sudden collapse of the beam. This failure occurred without fully developing the flexural capacity of the strengthened section. The third type of epoxy tested was a two-component rubber toughened epoxy, with tensile lap shear

strength of 14-15 MPa. The test specimen reached an increase in ultimate load of 100% over the control beam. There was no visible cracking up to 70% of the ultimate load and failure was the result of delamination of a strip of concrete just above the bond line, along the full length of the beam. The fourth adhesive was the most rigid of all the epoxies tested. This resulted in a very brittle and sudden failure which is caused by plate separation due to the formation of flexural cracks (Saadatamanesh and Ehsani 1990).

Saadatmanesh and Ehsani (1991) attempted to investigate the static ultimate strength of five rectangular RC beams and one Tee beam strengthened by gluing GFRP plates to their tension flanges. All beams were simply supported on a clear span of 4.57m and were subjected to four-point bending. The five rectangular beams (A through E) were 205 x 455 mm in cross section and were reinforced with 2 12.7mm bars on the top and different reinforcement ratios at the bottom to investigate the effect of steel ratio on the strength of the upgraded beams. The GFRP plates, used to strengthen all the beams, were 6mm thick by 152mm wide and 4.26m long. Beams A and B were typical beams strengthened with GFRP plate only. Beams C and D were held cambered while bonding the composite sheets to them in an upside down position. The results of the four-point bending showed an increase in the cracking load in excess of 100% over the predicted value for the control beam and an increase in excess of 400% over the predicted failure load of the control beam as well. The load was monotonically increased to failure with one cycle of loading and unloading. Failure of Beam A occurred by crushing of concrete in the compression zone while that of Beam B was initiated by debonding of the GFRP plate. Failure of Beams C and D occurred due to the concrete cover separation in between the GFRP-plate and the tension steel rebars. Beam E was only reinforced with the GFRP plate with no longitudinal steel reinforcement. This caused it to fail prematurely by large tension cracks. The T beam

(Beam F) had a flange size of 610mm x 75mm and a web size of 205mm x 455mm. It showed a significant increase in load and stiffness over the control specimen and failed due to debonding of the plate at the end.

The experimental program by Meier and Kaiser (1991) consisted of externally bonding carbon fiber reinforced plastic (CFRP) sheets to 26 reinforced concrete beams having 2m-span and one RC beam with 7m-span. The test specimens (150 mm by 250 mm by 2m) were reinforced with four 8 mm diameter bars (two in the compression zone and two in the tension zone of the beam) and the shear reinforcement was 6 mm bars spaced at 220 mm on center. It was determined that the use of a 3mm thick and 200mm wide CFRP sheet will result in 100% increase in ultimate load over the control beam. The deflection was expected to be only half of the control beam deflection. It was noted that in a typical under-reinforced section, the increase in the ultimate load was only 22%. The bonding of the pre-cracked beam with a CFRP sheet resulted in a uniform distribution of cracks along the full length of the member.

Rizkalla and Erki (1991) reported that several advantages exist for a combined bolted/bonded anchorage of externally applied CFRP sheets. The adhesive has the ability to minimize the fatigue problems caused by the bolt-type fasteners and can reduce or even eliminate the stress concentrations around the laminate bolt holes. The adhesive may also provide protection against any possible corrosive effects of the metal bolts. On the other hand, the bolts will resist peeling of the laminate and will allow for immediate loading of the member before the curing of the adhesive. It has been reported (Deblois et al. 1992) that this combination of bolted/bonded strengthening system showed different levels of success in this application.

Ritchie et al. (1991) tested a series of 16 under-reinforced concrete beams to investigate the effectiveness of external strengthening using different types of FRP plates. Glass, Carbon

and Aramid fiber reinforced laminates, along with steel plates, were bonded to the tension side of the beams using a two-part, rubber-toughened epoxy. All beams were of 6"x12" (152 mm by 305 mm) in cross-section and were 9' (2743 mm) long. Two beams were tested as control specimens and two were strengthened with steel plates while the rest were reinforced with the three types of FRP plates. The paper reported an increase in the initial stiffness and service load from 17 to 99% and an increase in ultimate strength of 40 to 97% for the FRP strengthened beams. Experimental failure did not occur in the constant moment region in many of the beams, despite attempts to provide some end anchorage to delay local shear failure. The ultimate load of the beams that failed in flexure was within about 5% of the predicted value. The beams with externally bonded plates exhibited another desirable phenomenon. The crack patterns shifted from having several widely spaced wider cracks, in the control specimens, to having many more closely spaced narrower cracks. This could be advantageous to improve the serviceability of such beams. Deflections of many of the beams exceeded an inch at failure. This corresponds to a very noticeable span/deflection ratio of less than a 100. It was concluded that the problem of shear stress concentration and plate end anchorage requires additional attention to avoid the undesirable separation failure mode at the plate ends.

Triantafillou et al. (1992) investigated the strengthening of flexural members using prestressed CFRP sheets. The unidirectional CFRP sheets were first pre-tensioned and then bonded to the tension face of the beam. Once the epoxy adhesive was fully cured, both ends were cut and the composite member was transformed into a prestressed element. Five beams of 70 mm by 120 mm by 1.2 m dimensions, were reinforced with a 4 mm or 6 mm bar in tension as well as 4 mm stirrups spaced at 40 mm on center for shear. The beams were tested in three point bending. The unstrengthened beams were reinforced with CFRP sheets at various prestressing

levels. The results of the flexural tests showed an increase of three to four times the ultimate load over the control beam. Failure of all prestressed beams consisted of diagonal cracks, which caused localized peeling-off and subsequent slipping of the CFRP sheets. All of the beams have then experienced some more increase in the load-carrying capacity until the concrete crushed in compression and/or the CFRP sheet fully debonded.

Meier et al. (1992) completed four-point bending tests on 6.0 m long Tee-beams with 260 mm by 340 mm web dimensions and 160 mm by 900 mm flange size. The beams were reinforced with four 26 mm bars on the tension face of the web, 10mm bars spaced at 45mm on center for shear and four 10 mm diameter bars in the flange. The externally strengthened beams had a 1mm thick by 260 mm wide CFRP sheet bonded to the tensile face of the web. The CFRP sheets were applied with and without prestressing. Experimental results showed an increase of 32% in the ultimate strength of beams with prestressed as well as non-prestressed CFRP sheets. The only difference between the two strengthening schemes was in the displacement at failure. The vertical deflection was the same in the control beam and the strengthened specimens without prestressing. On the other hand, the deflection was reduced by approximately 100% for beams strengthened with prestressed CFRP sheets.

Quantrill et al. (1996) carried out an experimental work on 10 small scale beams of 1m length and 100 x 100 mm cross-section. The specimen designated by B1 was a control beam. Four beams (B2-B5) were strengthened with GFRP plates and five beams (B6-B10) were strengthened with CFRP plates. Three types of anchoring systems were used in the experiment. A simple parametric study was carried out in which the plate area, plate aspect ratio, plate material and the method of plate end anchorage were varied. Experimental loads versus plate strains were reported along with the analytical results for fully and partially cracked sections.

Calculations for partially cracked sections were carried out using a linear model for concrete in tension as per the British standard (BS8110). The authors concluded that their experimental results are in good agreement with the partially cracked section instead of the fully cracked one due to the tension stiffening effect of the reinforcing steel and FRP plate.

Varastehpour and Hamelin (1997) conducted an experimental study on a series of three beams of 150 mm x 250 mm x 2.3 m dimensions. Two specimens were strengthened with CFRP plates and one beam was used as a control specimen. The results showed a 55% increase in stiffness with a significant loss of ductility.

In a study performed by Arduini and Nanni (1997a), experimental and analytical data on reinforced concrete (RC) beams strengthened with CFRP sheets was presented. In the experimental study, two different groups of rectangular concrete beams were investigated. One group represented short, shallow and wide beams and the other one characterized deep, narrow and medium length beams. In all, 18 rectangular specimens were tested. Nine of the specimens tested had a height to width ratio (h/b) of 0.5 (shallow beams) while the other nine had h/b ratio of 2.0 (deep beam). All but eight beams were pre-cracked before application of CFRP. The specimens were tested under four point bending. Besides beam geometry, three different variables were considered in this study. The first was the repair material, as two different FRP systems were evaluated. The second was the concrete surface preparation. Two methods of surface preparation were used, namely, sanding and sand blasting. The third variable was pre-cracking the beams versus leaving them virgin prior to loading them monotonically to failure. The experimental results showed a small increase in stiffness and significant increase in ultimate strength with the CFRP strengthened beams. This was true for both types of beams studied as well as both FRP systems used. Debonding and peeling of the FRP was a critical factor in terms

of ductility and FRP response. Many of the specimens experienced FRP de-bonding prior to
FRP rupture. Also, no significant difference in structural behavior was noted between the pre-
cracked and virgin specimens. The results of the experimental test correlated well with an
analytical model developed by Arduini.

In the experimental and analytical study performed by Norris, Saadatmanesh, and Ehsani
(1997), data and conclusions from flexural and shear tests on nineteen under-reinforced concrete
beams retrofitted with CFRP was presented. This flexural data was compared with an analytical
model developed by the authors. The analytical model was based on an incremental deformation
technique satisfying strain compatibility and cross section equilibrium. Shear analysis was done
using ACI equations modified to include the shear contribution of the FRP. Each of the 2.44 m
(96 in) flexural specimens had a rectangular cross-section of 127 mm x 203 mm (5 in x 8 in) and
a steel ratio of 0.0067. Thirteen of the specimens were over-reinforced in shear by closely
spaced mild-steel stirrups in order to enforce a flexural failure. The specimens were loaded at
the quarter points to provide a constant moment region in the center of the span. The shear
specimens were 1.22 m (48 in) with minimum steel shear reinforcement. Three types of FRP
systems were studied as well as different fiber orientations. The study showed that there was a
little difference between the fiber systems used and there was no difference between the pre-
cracked and the virgin specimens. The CFRP sheets provided an increase in strength and
stiffness to the control beams (20 –100% increase in ultimate strength). Stiffness was increased
more dramatically when fibers were placed perpendicular to pre-existing cracks in the pre-
cracked specimens.

In the analytical study performed by Arduini and Nanni (1997b), pre-cracked RC beams
of varying geometric and material properties were studied. The authors also varied the thickness

and mechanical properties of the FRP system in order to develop curves useful for designers. The model was verified against experimental data from earlier tests. This verification was mentioned but not presented. All analytical results were reported in terms of upgraded to original ultimate capacity and deflection ratios. The study looks at repairing for two separate conditions--stiffening and strengthening. In general, it was shown that the stiffening is always attainable. For a given FRP thickness, a stiffer FRP will provide better results. Likewise, for a given FRP, more layers will provide more stiffness. Strengthening of a beam is somewhat less reliable. The success of the repair is limited by: 1) the shear strength of the existing member, 2) mode of failure of the repaired system, and 3) deflection at the new service load. To truly increase the strength of the specimen, all of these limiting factors must be considered.

Spadea et al. (1998) tested four 5m beams of 140 x 300mm in cross section under displacement control. Beam designated as A3 was the control specimen while the other three (A3.1-A3.3) were bonded with CFRP plates on the tension face. The moment-curvature curves of their experimental work showed that the strength and ductility of the section can be increased and the bond slip can be minimized by providing external anchorage to the FRP plate. External steel U-wraps were used for this purpose. All the beams were tested under four-point bending over a span of 4.8m. The beams were extensively instrumented to monitor strains, deflection and curvature over the entire spectrum of loading to total failure and to determine the structural response of the composite beams. The results show that bonding a CFRP plate on the tension face of a RC beam without consideration of the end-anchorage stresses and the plate bond slip can lead to significant degradation in the structural response of the plated beam. Increase in load capacity of up to 70%, substantial regain of structural ductility and the transformation of a brittle failure into a more ductile failure were improvement reported as result of the use of the

steel U-wraps. However, it is uneconomical to adopt their anchoring procedure in the field to strengthen existing beams.

The study performed by Shahawy and Beitelman (1999) shows the results of an experimental work on RC T-beams. The beams were tested under static and fatigue loading conditions. Ten beams were tested statically and six were tested under fatigue. The T-specimens were 445 mm (17.5 in) deep with an 89 mm (3.5 in) thick by 584 mm (23 in) wide flange. Two layers of tension steel were used as well as one layer of compression steel in the flange. The specimens were tested under four point bending with the loads being applied at the third points. The fatigue loading was sinusoidal and varied from 25% to 50% of the ultimate capacity of the specimens. Three different wrapping methods for the FRP were used. The specimens were either not plated, plated by FRP applied to the bottom face of the web only, or fully wrapped where the entire web of the specimen was wrapped. Besides this, various numbers of layers were used in the strengthening procedures. The experimental results correlated well with a two-dimensional finite element analysis. The results show that RC beams can be strengthened for both static and fatigue. From the static tests, fully wrapped specimens performed better than the plated specimens. Delaminations that occurred in the plated specimens did not occur in the fully wrapped specimens. In terms of fatigue, the specimens were able to withstand up to 2 million load cycles without failure.

El-Tawil, Ogunc, Okeil, and Shahawy (2001) presented the results of an analytical study on RC T-beams. The study attempted to correlate data from two separate static and fatigue tests on RC specimens strengthened by CFRP with an analytical model based on strain compatibility. Factors accounted for in the static model include strain hardening of the steel reinforcement, and tension stiffening of the concrete. For the fatigue model, time dependent effects and material

13

degradation were also accounted for. The study showed that the strain compatibility model could accurately predict the static and fatigue behavior of the specimens. The study also gave recommendations on shear design using FRP reinforcement. Based on their data, it is best to limit the stress in the steel reinforcement to 0.85 times the yield stress.

Fanning and Kelly (2001) outlined the results of an experimental study performed on ten 3 m long (9.8 ft) specimens. The beams were 155 mm (6.1 in) wide by 240 mm (9.45 in) deep. Three 12 mm bars were used for tension reinforcement and two 12 mm bars were used for compression reinforcement. Flexural strengthening was performed using the Sika CarboDur S strengthening system. The experimental results were compared with the results of an analytical model. The test showed that stiffness was increased by as much as 40% over the control specimen. A 70% increase in ultimate flexural capacity was also noted. The crack pattern of the strengthened specimens was significantly different as they were fewer and farther apart. The effectiveness of the strengthening system was lowered when the CFRP plates were shortened. The shorter the plates, the earlier the premature failure observed due to cover separation.

Wang and Restrepo (2001) showed the results of an analytical and experimental study on the behavior of RC T-beams strengthened for flexure with staggered CFRP. The analytical model builds upon the work done by Arduini and Nanni (1997b) by taking into account the effects of diagonal tension cracking and consideration of stresses at the concrete-FRP interface. The experimental study was performed on seven 5 m (16.4 ft) long T-beams. Unidirectional CFRP plates were used as longitudinal reinforcement while unidirectional GFRP plates were used as transverse reinforcement and anchorage devices. The specimens were loaded under six-point loading with load being applied every 1000 mm (39.4 in) along the span. The strengthened specimens showed an increased stiffness in the service load range. A significant increase (up to

25%) in the ultimate flexural capacity of the strengthened specimens was also seen. The

analytical model based on strain compatibility accurately predicted the load behavior of both the

strengthened and unstrengthened specimens. There was also good agreement between the

predicted and measure strains on the plate surfaces.

Chapter 4

Experimental Program

This chapter describes the properties of the studied specimens as well as repair and strengthening methods used. The pre-existing reinforcement details, FRP repair, and experimental setups and procedures for flexural and shear tests are covered.

4.1   Specimen Properties

Besides geometry and reinforcement details, this section describes the properties of the constituent materials that make up the specimens. A written account of the pre-existing damage to each specimen is also included in this section.

4.1.1   Specimen Geometry and Reinforcement

As noted earlier, each specimen represented one-half of a 1.83 m (6 ft) wide, 12.2 m (40 ft) long double-tee beam. Therefore, each single-tee specimen was 915 mm (3 ft) wide with the stem centered on the flange of the tee. The flange was 125 mm (5 in) deep while the overall depth of the beam was 585 mm (23 in). The web was tapered so that the width at the top of the web was 140 mm (5.5 in) and the width at the bottom of the web was 115 mm (4.5 in). A 100 mm (4 in) diameter round fillet connected the web and flange while a 13 mm (0.5 in) diameter round fillet smoothed the corners of the web's bottom.

The primary flexural reinforcement consisted of four (4) 13 mm (1/2 in) diameter prestressed tendons. The tendons were harped to a single layer at mid-span with 38 mm (1.5 in) of clear cover from the bottom of the web. There were also two layers of "compression" mild steel rebar in the flange. This consisted of five 9 mm (#3) bars spaced non-symmetrically about

the centerline of the specimen. There were also two layers of 13 mm (#4) rebar serving as transverse reinforcement in the flange.

The shear reinforcement in each specimen consisted of single-legged 16 mm (#5) mild steel rebar spaced evenly at 255 mm (10 in) on center throughout the length of the specimen. The bar was originally an up-side-down U-shaped stirrup with each leg extending into a web of the double-tee beams. The bars terminated 125 mm (5 in) from the bottom face of the web leaving no confinement around the prestressing tendons in the middle third of the beam. The cross section details for the specimens can be seen in Figure 4.1.
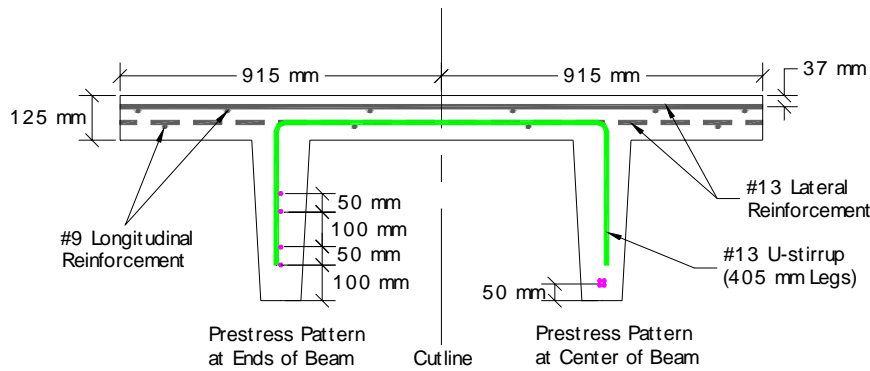
FIGURE 4.1: Cross-Section Details of Specimens

4.1.2   Pre-Existing Damage

After the beams were saw cut into the six specimens, the pre-existing damage on all of the specimens was recorded. The damage included large areas of spalled concrete at the bottom of the web as well as extensive flexural and shear cracking. Crack maps were drawn for each specimen and can be seen in Appendix A. The following notes are made about the condition of each specimen.

Specimen 1: This specimen was in the worst condition of all five tested. Large, wide shear cracks were found in the outer third parts of the specimen while many

flexural cracks were in the middle of the span. Two prominent spalls were located at the bottom of the web 2.13 m (7 ft) on either side of mid-span.

Specimen 2: Shear cracks were found on one end of the specimen only. On this end, wide shear cracks were found until about 3.05 m (10 ft) from the end. One of the shear cracks located at about 915 mm (3 ft) from the end had developed a very large spall on the bottom of the web. The cracks changed more to flexural-shear cracks and pure flexural cracks closer to mid-span.

Specimen 3: This specimen had no major shear cracks or spalls but did have some wide flexural cracks in the middle half of the beam.

Specimen 4: Large prominent shear cracks dominated one end of this specimen. Towards the middle however, there were few flexural cracks with no major areas of spalling.

Specimen 5: This specimen had no shear cracks at either end. However, large flexural cracks existed in the middle 8 m (26 ft) of the specimen. Many of these flexural cracks had developed large prominent spalls where in some cases the bottom two layers of strand were exposed.

It is worth mentioning that Specimens *1* and *5* belong to the first double-T girder while Specimens *2* and *4* were cut from the second girder. The twin of Specimen *3*, taken from the third double-T, was shipped to the University of Missouri, Rolla for further testing under this project contract agreement.

4.1.3   *Material Properties*

Concrete strength for these specimens was determined by taking cores from the specimens after all testing was completed. The 100 mm (4 in) diameter cores were taken from

the flange and web where there were no prominent cracks or steel reinforcement. Results of the

core tests can be seen in Table 4.1 along with other material properties. The stress-strain

behavior in compression is based on the Hognestad Parabola (Park and Paulay 1975). The

concrete was assumed to carry tension to a stress of $6\sqrt{f'_c}$ with the stress strain properties being

linear-elastic until cracking. Tension stiffening of the concrete due to the presence of both steel

and FRP was also considered as a parameter in the analytical model. The stress in the concrete

was assumed to degrade linearly after cracking to a stress of zero at 20 times the cracking strain

(El-Tawil et al. 2001). The stress-strain curve for concrete can be seen in Figure 4.2 (a).

Table 4.1: Material Properties

Material	Young's Modulus E, GPa (ksi)	Ultimate Strain ε_u, mm/mm	Ave. Ultimate Strength f'_c or f_u, MPa (ksi)	Source
Concrete (Specimen 1)	31.5 (4500)	0.003	43 (6.2)	3 Cores (min.)
Concrete (Specimen 2)	33.6 (4800)	0.003	49 (7.1)	3 Cores (min.)
Concrete (Specimen 3)	33.3 (4750)	0.003	48 (6.9)	3 Cores (min.)
Concrete (Specimen 4)	N/A	0.003	N/A	N/A
Concrete (Specimen 5)	N/A	0.003	65 (9.4)	3 Cores (min.)
Prestress Strand	200 (28,500)	---	1,890 (270)	PCI Handbook
Existing Mild Steel	207 (29,000)	---	280 (40) *	Estimate
Carbon FRP	231 (33,000)	0.014	3,080 (440)	Coupon Test
NSM Rebar	207 (29,000)	---	420 (60) *	Tensile Test

* denotes yield stress

The prestressing tendons were assumed to be (270 ksi) strand. The stress-strain

properties were assumed to be similar to those of the PCI model adopted by the PCI Design

Handbook (PCI 2001). This stress-strain relationship is shown in Figure 4.2 (b). Prestress losses

were also estimated to be 26 % (See Appendix B for Loss Calculations).

A bi-linear stress-strain model was used for the pre-existing mild steel compression

reinforcement with a yield strength estimated to be 280 MPa (40 ksi). The model was assumed

to be linear elastic-perfectly plastic, as shown in Figure 4.2 (c).
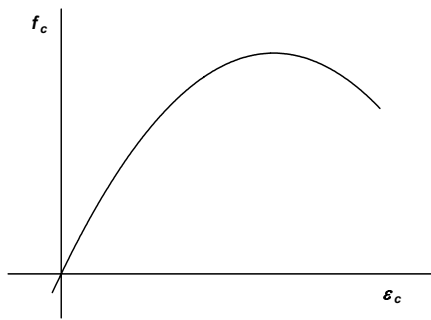
(a) Concrete stress-strain curve in compression
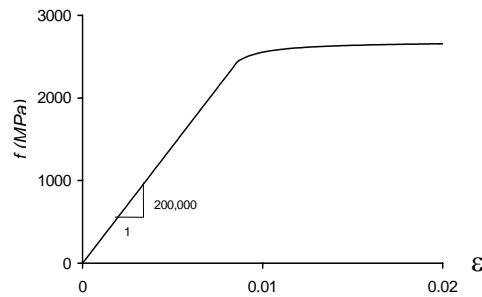
(b) Stress-strain curve for strands
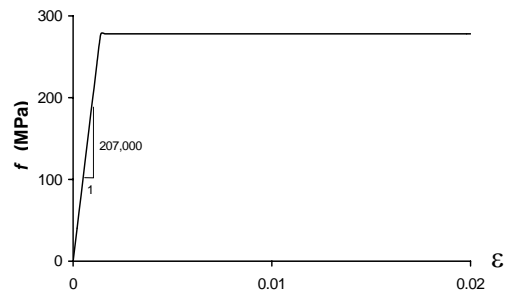
(c) Stress-strain curve for mild steel

FIGURE 4.2: Material Models

4.2   Repair and Strengthening Process

Specimen 1 was used as a control, so no repair was performed on it. Treatment of Specimens 2-5 was a multi-stage process in which the pre-existing damage was repaired and the bonding surface prepared properly to ensure an adequate bond between the FRP and concrete. The following sections will detail the repair steps.

4.2.1   Repair of Pre-Existing Damage

The first step in the repair process was to repair all areas of spalled concrete. First, wood forms were built around the damaged area. A small hole was left in the form and a high-strength epoxy grout was poured in until the spalled area was completely filled. The epoxy grout was then

allowed to cure overnight before the forms were taken off. The grout was made by mixing equal parts of medium grade sand and Unitex Type III D.O.T.

The next step in repairing the pre-existing damage was to epoxy inject all cracks on the surface of the webs. Plastic injection ports were drilled or glued on each crack. Several ports were put on each crack (typically spaced 150-200 mm or 6-8 inches apart) on both sides of the specimen. The cracks were then "buttered" by sealing them with a high-strength non-sag epoxy (Unitex Pro-Poxy 300). The sealing epoxy was spread to a minimum of 6 mm (0.25") thick and 50 mm (2") wide per ASTM specification (See Appendix C). This was allowed to cure for 24 hours before epoxy was injected into the cracks. The injected epoxy was pumped into the bottom most port for each crack at a pressure of 140 kPa (20 psi). As the cracks were filled, epoxy bled out of the higher ports and these ports were immediately sealed. Epoxy injection process was the most time consuming of all repair and strengthening activities as it took approximately four working days to epoxy inject one specimen.

4.2.2 Strengthening Process

Since Specimen 1 was left unrepaired, strengthening only needed to be done on Specimens 2-5. Specimens 2-4 were strengthened with only CFRP sheets while Specimen 5 incorporated near surface mounted (NSM) rebars as well as the CFRP sheets. The procedures followed to strengthen the specimens are detailed below:

4.2.2.1 CFRP Placement

Placement of the CFRP sheets was a three step wet lay-up process. Since it is a wet lay-up process, all materials are put on before the epoxy is allowed to cure. The application of the materials is very simple and requires no specialized tools. The steps in the process are outlined as follows:

Step 1. *Clean the Bonding Surfaces of Specimen*. All hardened epoxy from the epoxy injection process was removed from the specimen with an air hammer. Then the entire web was sandblasted to remove all adhering dirt. This left a clean etched finish on the surface of the webs.

Step 2. *Surface Preparation.* Prior to the placement of the CFRP sheets, a primer was used on the bonding surface using a paint roller. The primer was immediately followed by epoxy putty that was used to fill in any small "bug holes" on the concrete surface.

Step 3. *CFRP Placement*. Before the putty and primer were allowed to cure, the first layer of epoxy resin was applied to the specimen. Once again, it was applied using only a paint roller. Next a layer of fiber was pressed into the resin with a ribbed aluminum roller. Use of the roller was important because it pushes air out from underneath the fiber and prevents large air pockets from forming. Next another layer of resin is applied over the fiber. This process continues until all layers of fiber are put on. It is important to note that each layer must be place before the previous layer is allowed to fully cure. This helps ensure a continuous bond between all of the layers. Photos of this process can be seen in Appendix C. Figure 4.3 is schematic of a typical wet lay-up.
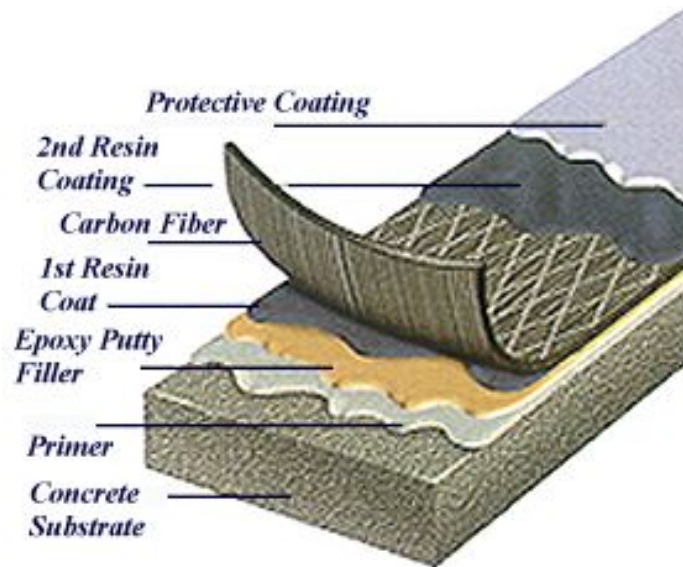
FIGURE 4.3: CFRP installation sequence (*adapted from www.mbtaus.com*)

4.2.2.2 Near Surface Mounted Rebar Placement

Placement of the NSM rebar for Specimen 5 was performed before the placement of the FRP sheets. The process of mounting the rebar began by cutting grooves in the sides of the web using a diamond tipped saw blade on a hand rotary saw. First two parallel lines were cut to a depth of 25 mm (1 in) along the section of the beam where the rebar was to be placed. Next, the material between the two lines was hand chiseled out. Since a 19 mm (#6) rebar was used, a 25 mm (1 in) groove was prepared. Figure 4.4 shows a drawing of the typical NSM rebar placement.

Once the groove was made, a non-sag structural epoxy was hand-placed into the grooves filling them approximately half-full. The rebar was then pushed into the groove making sure to get a layer of epoxy between the bar and all three sides of the groove. Epoxy was then spread over the bar and the surface worked to a smooth finish. Photos of this process can be seen in Appendix C.
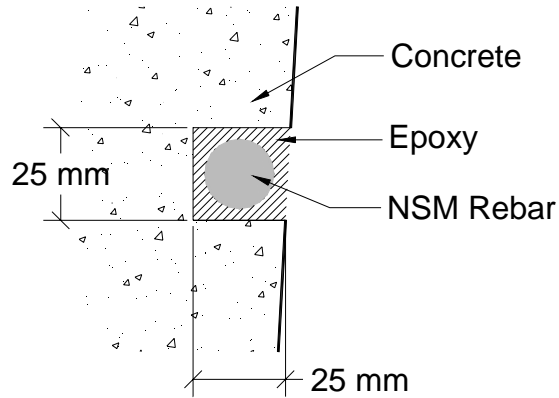
FIGURE 4.4: Layout for NSM Rebar Placement

4.2.3 *Properties of Repair and Strengthening Materials*

All epoxy used for injection, spall repair, and NSMR were supplied by the Unitex

Corporation of Kansas City, Missouri. Unitex *Pro-Poxy 50* was used for injection. This epoxy

has a maximum tensile strength of 50 MPa (7 ksi) with a maximum elongation of nearly 3%.

The grout used to repair the spalls was Unitex *Pro-Poxy Type III D.O.T.* mixed with equal parts

medium grade sand. The tensile strength of the epoxy was 18 MPa (2.6 ksi) with an elongation

of nearly 50%. The epoxy used for NSM re-bar and also for "buttering" the cracks was Unitex

Pro-Poxy 300 Fast. It was a non-sag epoxy typically used for anchoring bolts in concrete. The

technical data for all three materials can be found in Appendix D.

The CFRP materials were provided by Master Builder's Technologies of Cleveland,

Ohio. The Master Builder's CF-130 system was chosen for this project. The fibers were

unidirectional with a thickness of 0.165 mm (0.0065 in). The material was linear-elastic up to

failure, in the fiber direction, with a reported elastic modulus of 231 GPa (33,000 ksi) **based on**

the fiber area and an ultimate tensile strain of 0.017 mm/mm. The technical data for all

constituents of the M-Brace system can also be seen in Appendix D.

4.2.3.1 Coupon Tests on CF-130 System

To verify the properties of the composite system, tension tests (as per ASTM D-3039) were performed. Tension coupons were made from the same materials used on the concrete specimens. The coupons were 25 mm (1 in) wide by 230 mm (9 in) long and two layers thick with the fibers running parallel to the longitudinal direction of the test coupon. GFRP tabs were machined and bonded to the ends of the test coupons to avoid failure at the grips. Strain gages were mounted in the middle of each specimen parallel to the fiber orientation. Strain and load data for each specimen were acquired as the specimens were loaded to failure. The results show a similar modulus of 231 MPa (33,000 ksi), based on the fiber area, as that listed by the manufacturer but a noticeably lower ultimate strain of 0.014 mm/mm. These values were used in all subsequent calculations. The data from the coupon tests can be found in Appendix E.

4.3 Test Setup and Procedures

Four different setups were used for the various tests run on the Graham County beams. This section will detail the different setups and also the procedures used for each test. Included will be the setups and procedures for both static and fatigue testing in flexure as well as the static testing of shear capacity. All tests were performed in the 2200 kN (500 kip) capacity Haven's-Steel Structural Load Frame at the CISL facility at Kansas State University.

4.3.1 Flexural Tests

For flexural tests of Specimens 1-4, the beams were simply supported at 305 mm (12 in) from each end giving a test span of 11.6 m (38 ft), as shown in Figure 4.5. A hydraulic actuator was used to load the specimens at mid-span and the load was distributed across the entire flange using a transverse spreader beam. A gypsum cement (Hydro-cal) was used in the interface between the spreader beam and the specimen to provide a smooth loading surface. Two 255 mm

(10 in) linearly variable displacement transducers (LVDTs) were positioned (one on each side of the flange) to measure midpoint deflection during loading. The deflections reported herein are the average of these two readings.
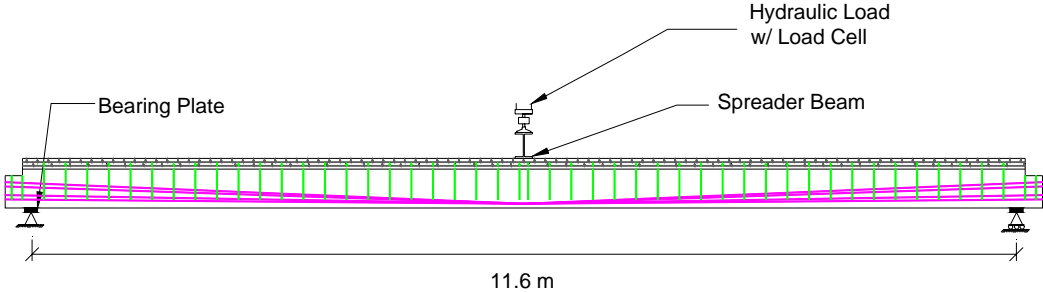
FIGURE 4.5: Flexural Test Setup for Specimens 1-4

The flexural test setup for Specimen 5 incorporated a longitudinal spreader beam to apply the load symmetrically about mid-span in four-point bending. Once again the beam was simply supported and the load was applied hydraulically at mid-span of the spreader beam. Deflection readings were obtained using two LVDTs, one on each side of the flange. The test setup for Specimen 5 can be seen in Figure 4.6.
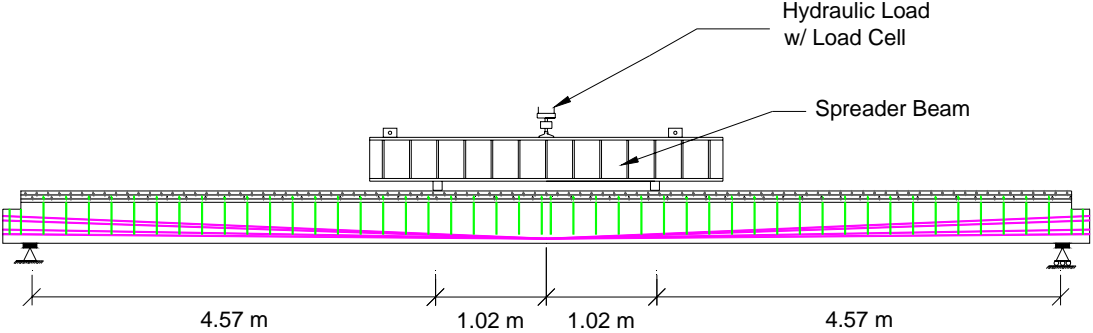
FIGURE 4.6: Flexural Test Setup for Specimen 5

4.3.1.1 Flexural Static Tests

Specimens 1-3 were all tested statically to failure. The beams were loaded monotonically at a load rate of approximately 6.67 kN/minute (1500 lbs/minute) with load and deflection readings taken at 1.11 kN (250 lbs) increments.

4.3.1.2 Flexural Fatigue Tests

Specimens 4 and 5 were tested for fatigue behavior. Sinusoidal cyclic loading was used for both specimens at a frequency of 0.5-0.75 Hz. *Following simple beam calculations*, the loads applied to each specimen produced an upper level moment at mid-span of 262 kN-m (197.5 kip-ft) and a lower level moment of 85.8 kN-m (64.25 kip-ft) (including the dead load of the specimen and spreader beam). The upper level represents the unfactored moment caused by the total dead load plus an HS-20 live load. The lower limit represents the total unfactored dead load moment including the application of a 1.2 kPa future wearing-surface. The hydraulic actuator load range for Specimen 4 was 6.67 kN (1.5 kips) to 68.9 kN (15.5 kips) while the hydraulic actuator load range for Specimen 5 was 1.11 kN (0.25 kips) to 77.9 kN (17.5 kips).

To determine if there were changes in stiffness of the specimens during the fatigue cycling, readings of load, deflection, and strain were taken periodically during static loadings. During the static loadings, the specimens were loaded monotonically at a rate of 6.67 kN/minute (1500 lbs/minute) to the same upper load level used for the cyclic loading. During the static loadings, data was taken at 1.11 kN (250 lbs) intervals. The load was then held at the maximum value for a three minute time period with readings taken periodically. Finally, the beam was unloaded gradually at a rate of 6.67 kN/minute (1500 lbs/minute) once again with readings taken at 1.11 kN (250 lbs) intervals.

4.3.2 *Shear Tests*

To maintain consistency in specimen properties and to get the most use out of the limited number of specimens available, the beams used in the flexural tests were also used for the shear tests. Each beam was cut in half near mid-span after the flexural test and each half was tested in shear. Two different setups were used for the shear tests. Both setups consisted of a 4.88 m (16 ft) simply supported span length with a hydraulic load applied at 1.22 m (4 ft) from the bearing point at the undamaged end. LVDTs were placed on both sides of the flange to measure deflections at the loading point. One setup incorporated a 0.61 m (2 ft) overhang on the undamaged end while the other setup had no overhang. The specimens for these tests are labeled as OH (overhang) or NOH (no overhang) throughout the remainder of this report. Figure 4.7 shows the typical setup for the shear tests. The flexural failure of Specimen 5 was such that a 4.88 m (16 ft) span could not be used for the shear tests. Therefore, the span for the shear tests for Specimen 5 was reduced to 4.27 m (14 ft) with the load point at 1.07 m (3.5 ft) from the undamaged end. Also, both halves were tested as no overhang (NOH) specimens.

The purpose of these two setups was to (1) investigate the effect of the CFRP wraps on web shear cracks that develop into the transfer length of the prestressing strands and (2) to determine the increase in shear capacity provided by transverse CFRP reinforcement. For beams that are not strengthened with external reinforcement, a web shear crack that extends into the transfer length can cause an immediate bond-slip failure of the prestressing strand (Russell and Burns, 1993). For the NOH specimens, the load was positioned close enough to the end of the beam to enable this type of failure. For the OH specimens, the transfer length (assumed to be 50 strand diameters) was not within the loaded span in order to prevent a bond failure from

occurring. Investigation of the NOH beams was used to determine if the transverse CFRP wraps

would help prevent bond-slip failures in damaged prestressed beams.

Load Point

3.66 m   1.22 m

(a)

Load Point

3.66 m   1.22 m   0.61 m

(b)
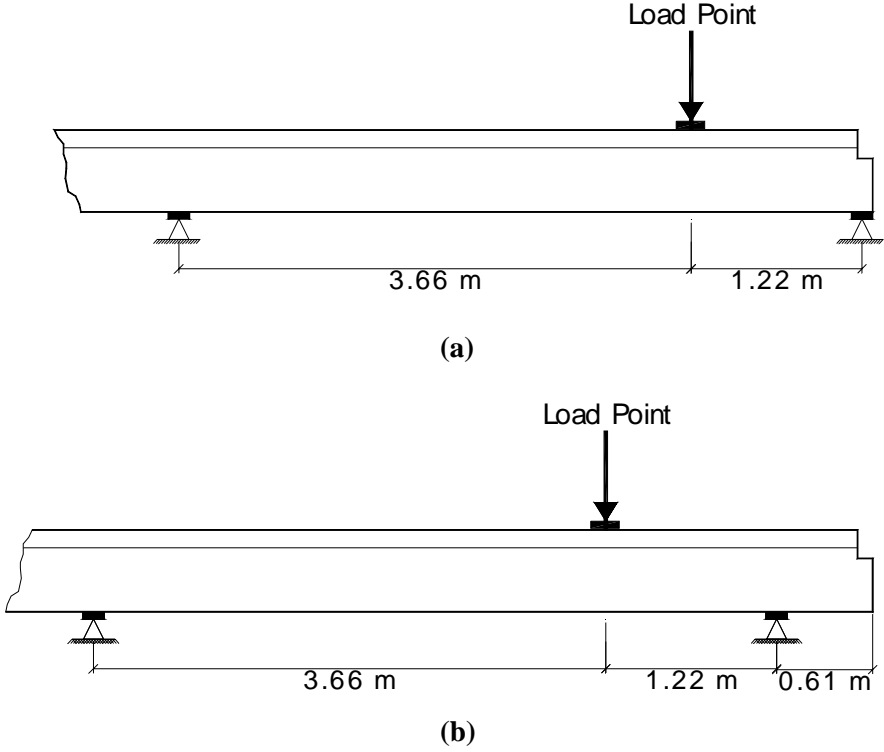
FIGURE 4.7: Typical Shear Test Setup (a) No Overhang (NOH) (b) With Overhang (OH)

Chapter 5

Analysis and Design

To insure that the strengthened specimens behave as expected, analytical models were developed to compare with the experimental results. For flexural analysis, the method of strain compatibility along with a moment curvature analysis was employed. Shear analysis was done using AASHTO Standard Specifications along with ACI code. These methods were also used to perform design calculations for CFRP reinforcement.

5.1   Flexural Analysis

Strain compatibility is often used for flexural analysis and design of prestressed concrete members (Nilson, 1987). However, because of its generality, it can be easily implemented in sectional analysis regardless of the type of reinforcement used (mild steel, FRP, etc.) provided that the perfect bond assumption applies. The accuracy of the model is highly dependent on the material models used. Thus, if the material models chosen can predict their actual response, the accuracy of the analysis is expected to be high. The material models detailed in Chapter 4 were used for strain compatibility calculations.

5.1.1   Strain Compatibility

The theory of strain compatibility is based on classical beam theory that plane sections prior to bending will remain plane during bending. In other words, for a given section in a beam, shear deformation is considered insignificant and a linear strain distribution exists at all load levels as shown in Figure 5.1. The strain at any depth in the beam can then be described in terms of two unique parameters. In this case, the two parameters are the slope of the line or curvature (ϕ) and the depth to neutral axis (c).
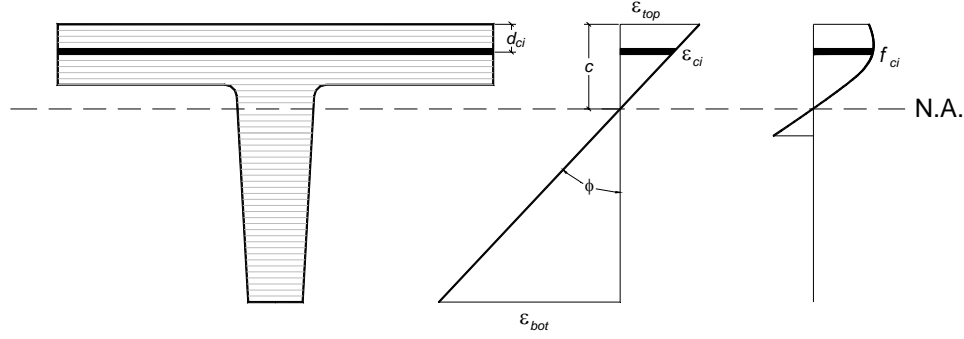
FIGURE 5.1: Strains and Stresses in Concrete Layers

Each section of the concrete beam can then be discretized, or broken down into a finite number of layers. The strain in each layer can be determined using the two parameters given above.

$$\varepsilon_{ci} = \phi(d_{ci} - c) \tag{5.1}$$

Knowing the strain, the stress in that layer of concrete can be determined. The stress is calculated as:

$$
f_{ci} =
\begin{cases}
f'_c\left(\dfrac{2\varepsilon_{ci}}{\varepsilon_0} - \left(\dfrac{\varepsilon_{ci}}{\varepsilon_0}\right)^2\right) & \text{for } \varepsilon_{ci} \leq 0 \\[3mm]
E_c\varepsilon_{ci} & \text{for } 0 < \varepsilon_{ci} < \varepsilon_{cr} \\[3mm]
f_R - \dfrac{f_R}{19\varepsilon_{cr}}(\varepsilon_{ci} - \varepsilon_{cr}) & \text{for } 20\varepsilon_{cr} > \varepsilon_{ci} \geq \varepsilon_{cr} \\[3mm]
0 & \text{for } \varepsilon_{ci} \geq 20\varepsilon_{cr}
\end{cases}
\tag{5.2}
$$

where ε_o is the strain corresponding to f'_c, ε_{cr} is the cracking strain of concrete and f_R is the modulus of rupture of concrete. The force in that layer of concrete can be found by multiplying the stress in the layer by the cross sectional area of the layer, or:

$$F_{ci} = f_{ci}b_{ci}t_{ci} \tag{5.3}$$

For the various layers of mild steel reinforcement, the same process can be done. Assuming that the bond between the steel and the concrete is adequate, the strain at the depth of the steel layer should be the strain in the concrete at that depth. Thus, the strain in a given mild steel layer can be found by:

$$\varepsilon_{si} = \phi(d_{si} - c) \qquad (5.4)$$

Assuming a linear elastic to perfectly plastic behavior for the steel in tension and compression, and knowing the cross-sectional area of the steel in that layer, the stress and force in the mild steel can be found as follows:

$$f_{si} = \begin{cases} E_s \varepsilon_{si} & \text{for } \varepsilon_{si} \leq \varepsilon_y \\ \\ f_y & \text{for } \varepsilon_{si} > \varepsilon_y \end{cases} \qquad (5.5)$$

$$F_{si} = f_{si} A_{si} \qquad (5.6)$$

Because the prestressing reinforcement has an initial tension due to the prestress force, it must be handled differently than the mild steel reinforcement. There are three components of strain in the prestressing strand and only one component varies with c and ϕ. The first component is the strain in the strand due to the prestress force (accounting for all losses). The second component is the strain to decompress the concrete at the level of the strand. The third component is developed due to the applied loading, which is the one that varies with strain distribution. The three components are calculated for each prestressed strand layer as follows:

$$\varepsilon_1 = \frac{P_{se}}{E_p A_p} \tag{5.7}$$

$$\varepsilon_2 = \frac{P_{se}}{E_c A_c} + \frac{P_{se}(e_{pi})(e_{avg})}{E_c I_c} \tag{5.8}$$

$$\varepsilon_3 = \phi(d_{pi} - c) \tag{5.9}$$

$$\varepsilon_{pi} = \varepsilon_1 + \varepsilon_2 + \varepsilon_3 \tag{5.10}$$

The stress can then be calculated using the guidelines found in the PCI Design Handbook, while the force is found by multiplying the stress by the cross sectional area.

$$f_{pi} = \begin{cases} E_p \varepsilon_{pi} & \text{for } \varepsilon_{pi} \leq 0.0086 \\ 270 - \dfrac{0.04}{\varepsilon_{pi} - 0.007} & \text{for } \varepsilon_{pi} > 0.0086 \end{cases} \tag{5.11}$$

$$F_{pi} = f_{pi} A_{pi} \tag{5.12}$$

Special considerations must also be taken when determining the actual strains in the CFRP and since the strain in the FRP will generally not be the same as the strain in the concrete it is bonded to. This is because there is an initial strain in the concrete at time of placement. This strain is caused by the self-weight of the beam and prestress force, but in general all loads at time of placement must be taken into consideration. This initial strain can be calculated by:

$$\varepsilon_{initial} = \frac{-P_{se}}{E_c A_c} - \frac{-P_{se} e_{avg}(d_{FRPi} - c)}{E_c I_c} + \frac{M_{Load}(d_{FRPi} - c)}{E_c I_c} \tag{5.13}$$

The strain in the concrete at the level of the external reinforcement and the strain in the reinforcement can then be calculated as follows:

$$\varepsilon_{C/FRP} = \phi(d_{FRPi} - c)$$
$$\varepsilon_{FRPi} = \varepsilon_{C/FRP} - \varepsilon_{initial} \tag{5.14}$$

The stress and force in the reinforcement can be then be calculated knowing the constitutive relationship of the material and the cross-sectional area.

$$f_{FRPi} = E_{FRP}\varepsilon_{FRPi} \qquad (5.15)$$

$$F_{FRPi} = f_{FRPi}A_{FRPi} \qquad (5.16)$$

It is noted that the same procedure must be used when calculating strains for the NSM rebar. The only difference will be the different material behavior (linear-elastic to perfectly plastic) noted in Chapter 4.

After determining all of the forces in the various layers of concrete and reinforcement it is now necessary to impose equilibrium on the section. Since no external axial forces are applied to the beam, the sum of the forces in any section at all load levels should be zero.

$$\sum F = \sum F_{ci} + \sum F_{si} + \sum F_{pi} + \sum F_{FRPi} = 0 \qquad (5.17)$$

Finding this equilibrium is an iterative process. For a given value of strain on the top face of the concrete a trial value for c is selected. The curvature and all forces can then be calculated as above. If the forces in the section equal zero, then the trial value for c was correct. Otherwise, a new value for c is selected and forces are recalculated. This is iterated until the sum of forces equals zero. The moment capacity at this state of strain can then be calculated and associated with the curvature:

$$M = \sum F_{ci}(d_{ci} - c) + \sum F_{si}(d_{si} - c) + \sum F_{pi}(d_{pi} - c) + \sum F_{FRPi}(d_{FRPi} - c) \qquad (5.18)$$

By doing this for various levels of strain at the top face of the concrete, a unique moment-curvature relationship can be developed for this section.

5.1.2 *Moment Curvature Relationship*

The moment curvature method can then be used to develop a load-deflection behavior for the specimen. First the specimen is broken down into a finite number of elements, each element having uniform section properties. Given the load setup, a load is then applied to the specimen. Taking into account the dead weight of the specimen and the applied load, the moment in each element can be calculated by simple statistics. Knowing the moment curvature relationship of each element, a curvature can then be associated to each element for that load level. Deflections at various points in the span can then be calculated using the moment-area method. Doing this at different load levels provides the load-deflection characteristics for the specimen.

This entire procedure requires many iterations and in general many calculations. When the section properties remain constant throughout the specimen, only one moment curvature relationship needs to be developed. However, if section properties change from one element to the next, for example a non-prismatic concrete section or harped strand, many different moment curvature relationships need to be developed thus adding to the amount of calculation. For this reason, this process lends itself well to computer programs. For this study, a routine was developed using the spreadsheet program Microsoft Excel and Visual Basic macros.

5.2   Shear Analysis

Shear analysis was based on AASHTO Standard Specifications equations. The equations were modified to include the contribution of the CFRP to the shear capacity. The nominal shear strength can be calculated as:

$$V_n = V_c + V_s + V_p + V_f \tag{5.19}$$

where V_c and V_s are the shear capacity of concrete and steel respectively. V_p is the contribution from the harping of the prestressing strand. The contribution of the CFRP was taken from the M-Brace Design Guide (M-Brace, 1998) and calculated as:

$$V_f = \frac{A_{fv} f_{fe} d_f}{s_f} \leq 4\sqrt{f'_c} b_w d_{ps}$$

(5.20)

5.3 Flexural Design

The design of the CFRP reinforcement for flexural strengthening was adapted from the MBT M-Brace design guide and was also performed using the strain compatibility method. For the strengthened specimens, an increase of 53% of the original ultimate design flexural capacity was sought.

Based on the geometry of the specimens (narrow web) and the area of CFRP needed to strengthen them to this level, it was determined that five layers of CFRP would need to be placed on the bottom face of the web. The manufacturer warned against using more than three FRP layers during a single lay-up since gravity may pull the carbon fiber sheets off of the beam prior to the resin setting. Accordingly, a different lay-up geometry was employed. Instead of layering only on the bottom face, 305 mm (12 in) wide sections of CFRP were wrapped around the bottom of the web as in Figure 5.3. Using this method, only two layers of CFRP were deemed necessary to achieve the desired strengthening. It was also determined from strain compatibility that CFRP rupture was the controlling failure mode (i.e. the CFRP would reach its ultimate tensile strain prior to the concrete reaching a compressive strain of 0.003).
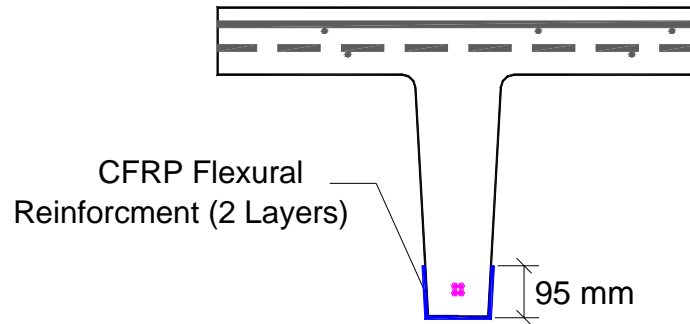
FIGURE 5.2: Section View of CFRP Flexural Reinforcement

5.4 Shear Design

A shear-friction approach similar to that depicted in ACI 318-99 Section 11.7.4 was used to design the CFRP stirrups for Specimen 3-5 (ACI, 1999). The first step was to determine the amount of tension force that was being transferred at the bottom of the beam from mid-span to the bearing point. Based on the strain compatibility the maximum tension force at mid-span due to CFRP rupture was 1090 kN (245 kips) and at the end the tension force is zero. Therefore, on average the amount of force transferred over the 6.10 m (20 ft) half-span is 180 kN/m (12.25 kips/ft). It was necessary to provide an opposing frictional force to this horizontal shear force. The normal force carried by the CFRP stirrups enabled this force, and can be quantified as follows:

$$\phi V_n = \phi A_{vf} f_F \mu \tag{5.21}$$

where f_F is the allowable tensile stress in transverse FRP (100MPa, 690 ksi), μ is the friction coefficient of the ACI shear friction model. Solving for A_{vf} showed that the required stirrup area must be greater than 220 mm^2/m (0.103 in^2/ft). To leave as much of the concrete face on the web uncovered as possible (since this would be desirable for future inspection of in-situ beams) two layers of 150 mm (6 in) wide CFRP stirrups spaced at 450 mm (18 in) on center

were used. This provided a stirrup area of 220 mm^2/m (0.104 in^2/ft). The elevation layouts of

CFRP reinforcement for Specimens 2-4 can be seen in Figure 5.3b. The layout for Specimen 5 is

shown in Chapter 6.

(a)

(b)
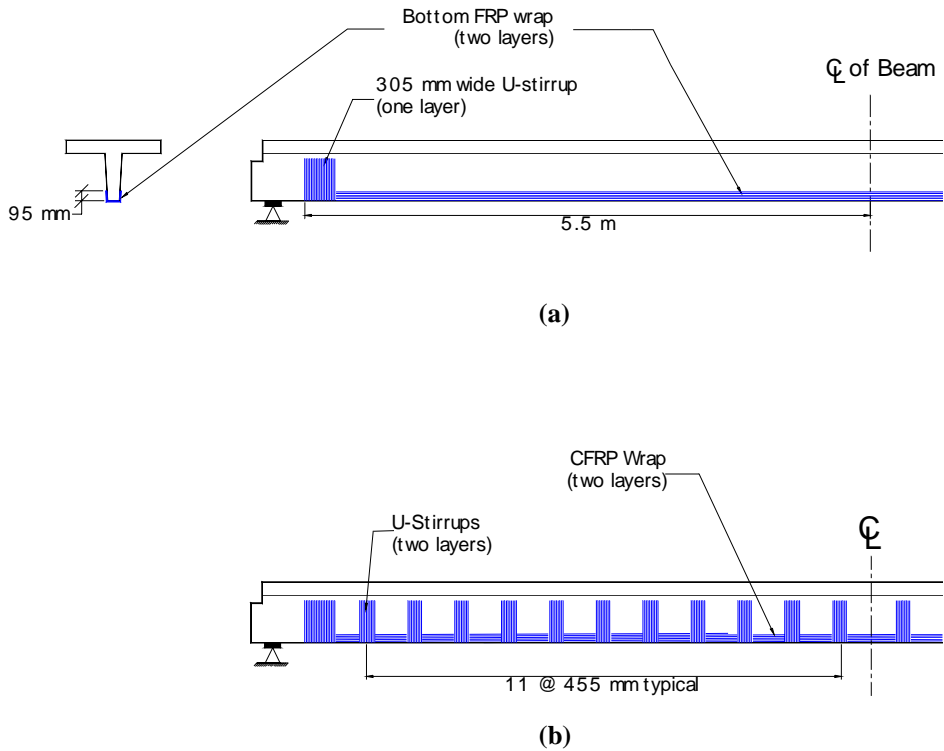
FIGURE 5.3: CFRP Layout for (a) Specimen 2 and (b) Specimens 3 and 4

Chapter 6

Discussion of Results

This chapter will detail the results of the experimental work done on the five prestressed concrete specimens as well as the comparison with the analytical results. Included will be sections describing the performance of the material in the static and fatigue flexural tests. Both types of shear tests will also be covered.

6.1   Flexural Tests (Static)

As previously mentioned, the first three specimens were tested for flexural capacity by being loaded statically to failure. The following sections will detail the results of the specimens individually. At the end of the chapter, the overall results of the three tests will be shown.

6.1.1   Results of Specimen 1

Specimen 1 was used as a control and tested without repair or strengthening. The specimen failed due to concrete crushing at the extreme compression fiber at an ultimate load of 130 kN (28.25 kips) and a corresponding mid-span deflection of approximately 305 mm (12 in). The strain compatibility model predicted a failure load of 115 kN (25.5 kips) with a mid-span deflection of 190 mm (7.5 in). The ductility of the specimen can be seen in the photo in Figure 6.1 (a). The ultimate flexural capacity, including the moment caused by the uniform self-weight of the specimen, was 440 kN-m (324 kip-ft). This was 11% higher than the theoretical value from strain compatibility and 28% larger than the design H-15 capacity. The theoretical and experimental load-deflection behavior of the specimen can be seen in Figure 6.1 (b).

Of all specimens tested and analyzed, this specimen had the worst correlation. The most notable difference between the analytical model and the experimental results is the 11% difference in ultimate moment capacity. Since geometry from this specimen as well as concrete strength was well documented, the most reasonable explanation for this difference is the possible higher strength of the prestressing strand. Strand specimens were later salvaged from specimens 4 and 5 for material static and fatigue testing. The tensile test yielded higher ultimate strength

| (a) | (b) |
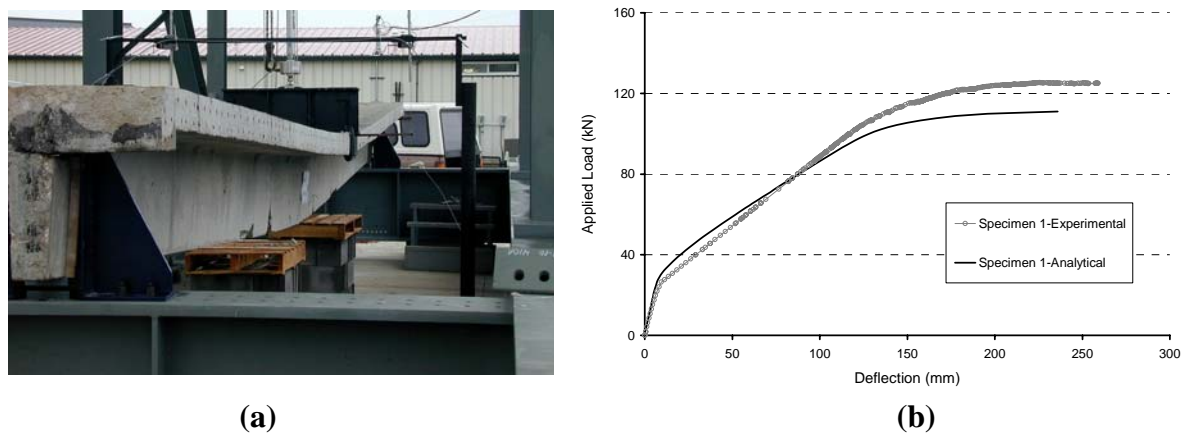
FIGURE 6.1: (a) Specimen 1 Near Failure (b) Load-Deflection Behavior of Specimen 1

than that assumed for the PCI 270 ksi standard strand (283.76 ksi). The experimental curve is compared to the PCI curve in Figure 6.2. It is evident that the difference between the two curves is very similar to that in Figure 6.1 (b).

6.1.2   Results of Specimen 2

Specimen 2 failed at an ultimate load of 160 kN (36 kips) corresponding to an ultimate moment capacity of 535 kN-m (393 kip-ft), at a deflection of 330 mm (13 in). The analytical model predicted a failure load of 161.5 kN (36.3 kips) at an ultimate deflection of 215 mm (8.5 in). The analytical model for this specimen was very accurate as it predicted the cracking load and the ultimate load very well (both within 1% of experimental results). The analytical and experimental load-deflection behavior of Specimen 2 can be seen in Figure 6.3 (a).
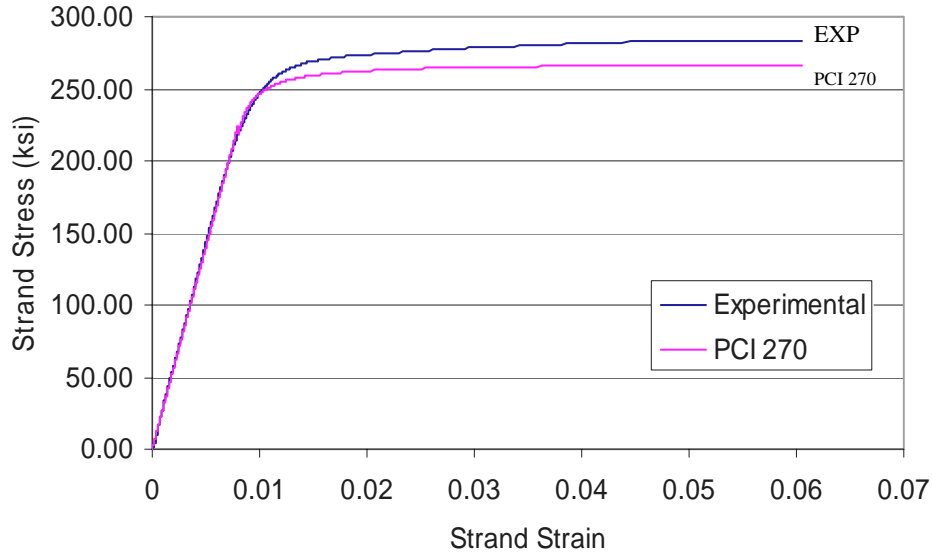
FIGURE 6.2: Comparison of Strand Experimental and Analytical Stress-Strain Curves

Specimen 2 failed when a horizontal shear crack occurred in the tension zone near mid-span (approximately 100 mm (4 in) from the bottom of the beam and extended longitudinally towards the support as shown in Figure 6.3 (b)). This failure was the result of two factors: the narrow web and the single legged stirrups that terminated at the level of prestress. As the beam was loaded the tension and compression forces at the bottom and top of the specimen, respectively, grew. Because the steel stirrups did not extend into the bottom of the beam where the large tensile force was being developed by the CFRP and the prestressing strand, the horizontal shear crack, once formed, was able to propagate along the entire length of the beam and divide it in two. Since the analytical model predicted rupture of the carbon fibers and CFRP rupture did not occur, full flexural capacity of this specimen may not have been reached.

The horizontal shear failure also explains the flat portion at the end of the experimental load-deflection curve. The horizontal shear crack did not form instantaneously. In fact, it took several second for it to propagate from mid-span to the end of the specimen. During this time, the load was held constant as the deflection increased.

41
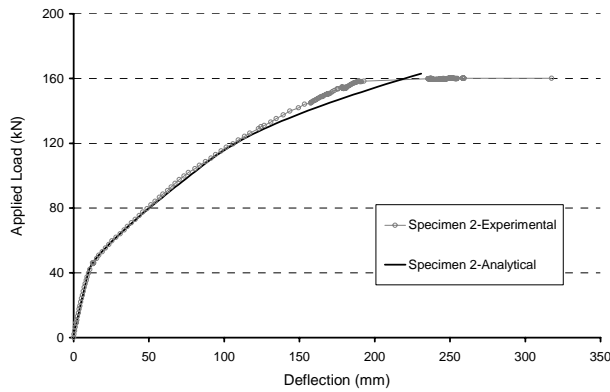
FIGURE 6.3: (a) Load-Deflection Response of Specimen 2 (b) Horizontal Shear Failure Mode

6.1.3   Results of Specimen 3

To insure that Specimen 3 failed by CFRP rupture, shear stirrups were included in the

design as mentioned in Chapter 5. This allowed Specimen 3 to reach an ultimate load of 162 kN

(36.5 kips), and an ultimate moment capacity of 540 kN-m (398 kip-ft). The ultimate deflection

was 345 mm (13.5 in). The load-deflection behavior can be seen in Figure 6.4 (a). This moment

capacity was 1% larger than the theoretical capacity calculated using strain compatibility, and

58% higher than the original H-15 design capacity of the unstrengthened specimen. Most

importantly, the beam reached failure by rupture of CFRP instead of horizontal shear, as the

analytical model predicted. Failure occurred as the bonded longitudinal CFRP between the

middle most two stirrups reached ultimate strain. At this point, the CFRP shattered (See Figure

6.4 (b)) and deflection increased instantaneously.
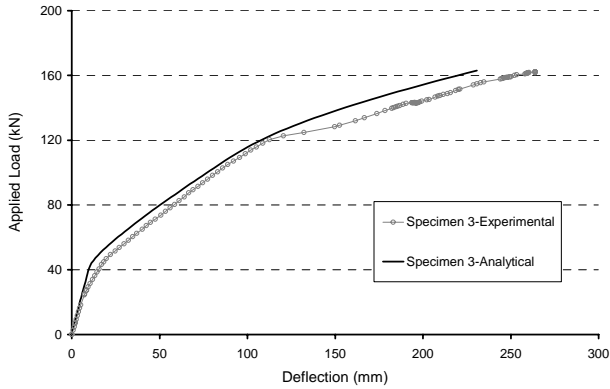
(a)

(b)

FIGURE 6.4: (a) Load-Deflection of Specimen 3 (b) CFRP Rupture at Mid-Span

The analytical model was the same used for Specimen 2. Though it predicted the failure

load and the cracking load very well some minor discrepancies appear upon closer inspection.

Two areas of "softening" were found in the experimental curve but not seen in the analytical

model. The first occurs at a load of about 20 kN (5 kips) until cracking at 40 kN (10 kips). This

is most likely attributed to early cracking of the epoxy injected cracks. The second softening

occurs near the yielding of the prestress strand at a load of 120 kN (30 kips). This was most

likely due to the sudden opening of a large flexural-shear crack between two FRP stirrups near

mid-span.
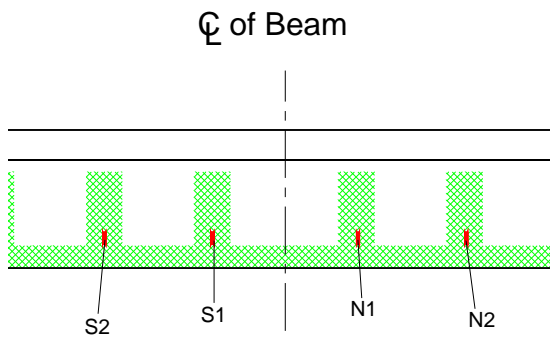
(a)
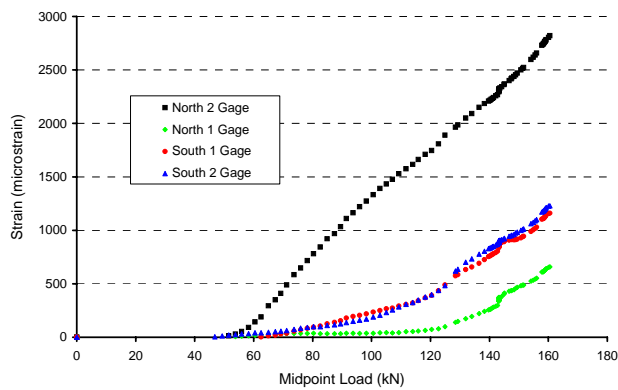
(b)

FIGURE 6.5: (a) Gages for Specimen 3 (b) Gage Data from Specimen 3

Additional experimental information was gathered from Specimen 3 as to the performance of the CFRP stirrups. To monitor the behavior of the CFRP U-stirrups, strain gages were placed on one side of the specimen on the middlemost four stirrups (two on either side of mid-span). The gages were placed along the stirrup axes, immediately above the longitudinal FRP layers as shown in Figure 6.5 (a). The U-stirrups presumably prevented the horizontal shear separation of the bottom CFRP reinforcement of the beam, as significant strain (and thus force) was developed in each stirrup gaged (See Figure 6.5 (b)). The highest strain was developed in the outer north stirrup (Gage N2) where a shear crack in the concrete extended below the FRP stirrup. The transverse strain in this stirrup reached about 94% of the design strain used in the shear-friction calculations.
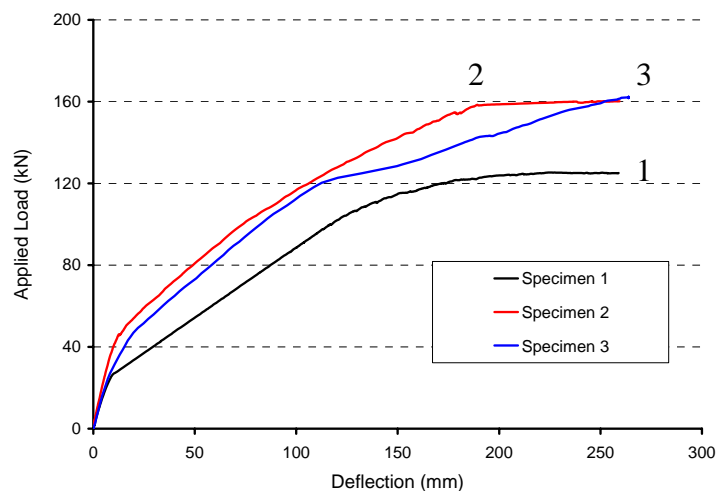
FIGURE 6.6: Comparison of Load-Deflection Behavior for Flexural Static Tests

6.1.4   Comparison of Specimens from Static Tests

A comparison of the three specimens tested statically for flexure shows that the overall behavior of the two strengthened specimens was different from the base specimen. CFRP strengthening allowed the moment capacity of Specimens 2 and 3 to increase 21.0% over

Specimen 1 amounting to a 28.5% increase in live load capacity. This was done without a compromise in ductility, as the total deflections for the three specimens were similar at failure. Only a small change in the initial stiffness was noted and this was most likely due to the fact that the cracks in Specimen 1 were not repaired. The load-deflection behavior of the three specimens can be seen in Figure 6.6.

For the most part, the structural behavior of Specimen 2 and Specimen 3 were very similar. The ultimate flexural capacity as well as the ultimate deflection was very close. The only significant difference was caused by the large shear crack that developed in Specimen 3 at 120 kN (27 kips) that caused structural softening. The major difference between the two specimens was the failure mode, with Specimen 2 failing because of horizontal shear and Specimen 3 because of CFRP rupture in the tensile zone. Table 6.1 shows a comparison of the three specimens.

TABLE 6.1: Comparison of Flexural Static Test Specimens

	Design Moment kN-m (kip-ft)	Theoretical Moment Capacity kN-m (kip-ft)	Actual Moment Capacity kN-m (kip-ft)	% Strengthened (Compared to Specimen 1)	% Strengthened above H-15 Capacity	Failure Mode
Specimen 1 *	340 (252)	400 (293)	440 (324)	0%	28%	Concrete Crushing
Specimen 2 **	520 (383)	540 (396)	535 (393)	22%	53%	Horizontal Shear
Specimen 3 **	520 (383)	540 (396)	540 (398)	23%	56%	FRP Rupture

* Design moment based on H-15 live load
** Design moment based on HS-20 live load

6.2 Flexural Tests (Fatigue)

Specimen 4 and Specimen 5 were both tested in fatigue. The following sections will detail the results of the specimens individually and overall results will be stated at the end.

6.2.1 Results of Specimen 4

Specimen 4 failed due to fatigue after 269,172 loading cycles. The failure mechanism was strand rupture due to fatigue. It appears that the strand ruptured in three distinct steps. The first strand ruptured after 268,159 cycles. At this point, a significant decrease in stiffness and

increase in deflections was noted during the static data test. The next strand fatigued after

268,966 cycles. Another significant decrease in stiffness was noted. The final failure occurred

during a static reading in which the specimen failed violently at a load of 53.4 kN (12.0 kips). A

plot of the load deflection behavior after various cycles can be seen in Figure 6.7 (a). Figure 6.7

(b) shows a comparison of the stiffness by showing only the ascending arm of the load-deflection

curves.
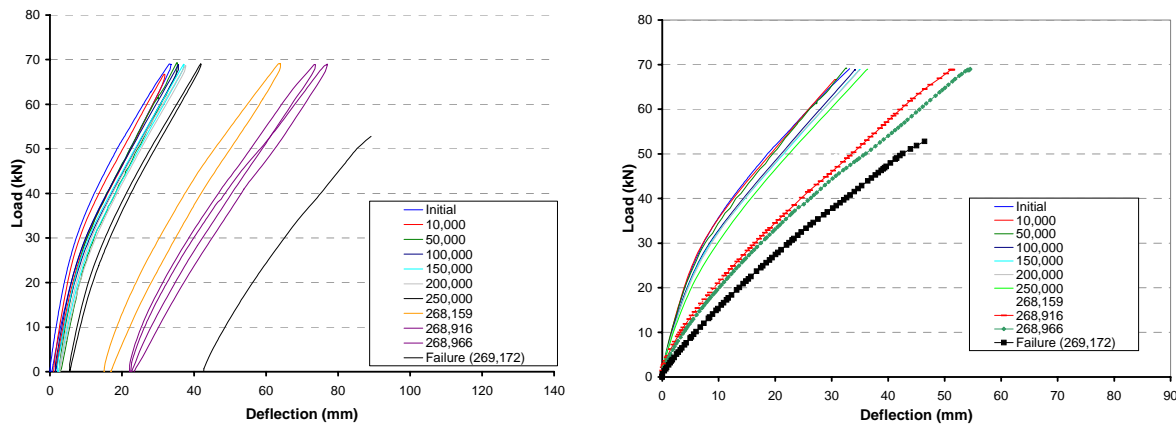
FIGURE 6.7 (a) Load-Deflection Cycles of Specimen 4
(b) Loading Cycles with Common Origin

Once again, the analytical model was used to correlate with the load-deflection behavior

of Specimen 4. Since the model does not account for creep or degradation of the materials due to

fatigue, it could only be compared to the initial loading. Good correlation was found between the

analytical model and the experimental data as shown in Figure 6.8.

The model was also used to determine the stress range in the strand at the failure point

(mid-span). Since the specimen failed because of strand fatigue, it is important to see what kind

of stress range was present. A plot of the stress in the prestressing strand versus theoretical

moment capacity can be seen in Figure 6.9. This plot can be obtained directly from the analytical

procedure described in Chapter 5. The plot shows that even with the CFRP strengthening, the

service moment was beyond the cracking moment and thus more stress was developed in the strand. The stress range in the strand was theoretically 262 MPa (38 ksi). The limit set forth by AASHTO at this point is 69 MPa (10 ksi).

FIGURE 6.8 Comparison of Experimental and Analytical Results for Specimen 4

Another contributor to the failure may have been the device used to hold down the strands at mid-span during casting of the specimens. The hold down device was composed of a 50 mm (2 in) wide piece of steel channel welded to a steel pipe. The channel was pushed down into the strand during original casting to provide the harped profile. Investigation of the device after failure showed areas where the strand may have been rubbing against it. This may have provided a large enough stress concentration to cause a failure. A photo of the hold down device can be seen in Figure 6.10.
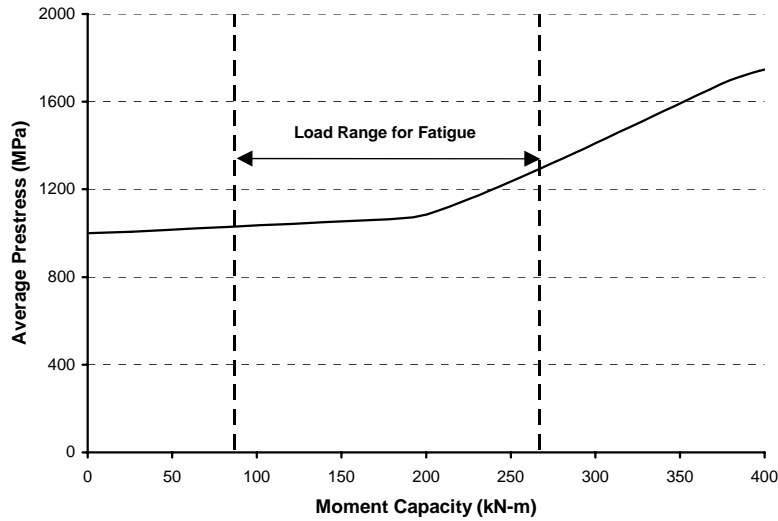
FIGURE 6.9: Stress Range in Strand of Specimen 4

FIGURE 6.10: Hold Down Device from Specimen 4

Fatigue tests were also performed on strand pieces taken from an uncracked region of Specimen 4. Two pieces were cut from the second strand profiling from top and the third one was extracted from the top strand. The three strands were loaded so as to provide the same stress range at which specimen 4 was cycled. The strands failed due to fatigue at 238,543 cycles, 247,128 cycles, and 200,880 cycles respectively. These results show that the high stress range was most likely the main contributor to the failure of Specimen 4.

6.2.2   Results of Specimen 5

Specimen 5 was tested to be sure the failure of Specimen 4 was due to the high stress range in the strand at mid-span and not the rubbing against the hold down device. To test this, additional reinforcement was added in the 1015 mm (40 in) around mid-span in order to increase stiffness and keep cracks from opening. Additionally, four-point bending (detailed in Chapter 4) was used to create a 2.44 m (8 ft) wide constant moment region symmetrically about mid-span. The combination of the load setup and the increased strengthening at mid-span allowed lower stress range in the repaired area with a higher stress range in the area between the repaired section and the applied load. If failure was induced outside the repaired area, it would be reasonable to assume that the high stress range in the strand was the main cause for failure of Specimen 4. If the failure was inside the repaired section, then the hold down device was more critical. Strain gages were applied to investigate the performance of the repair materials.

6.2.2.1 Details of Additional Reinforcement for Specimen 5

As mentioned in Chapter 4, Specimen 5 incorporated both CFRP and NSM rebar in the repair at midsection. The NSM rebar was applied first as the CFRP was placed on top of it. Two layers of rebar with two rebar each were put onto the sides of the web. The two layers were at a height of 90 mm (3.5 in) and 150 mm (6 in) respectively from the bottom of the web. The rebar were 1.52 m (5 ft) long placed symmetrically about the mid-span of the Specimen. Layout for the NSM rebar can be seen in Figure 6.11.
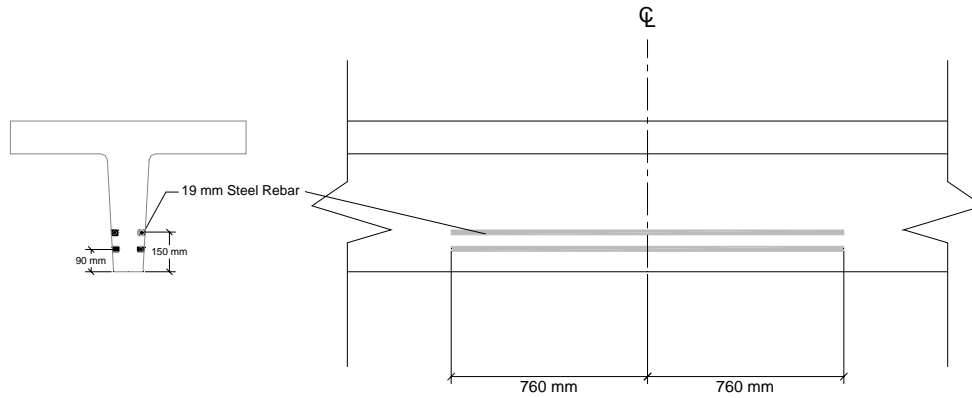
FIGURE 6.11: NSM Rebar Layout for Specimen 5
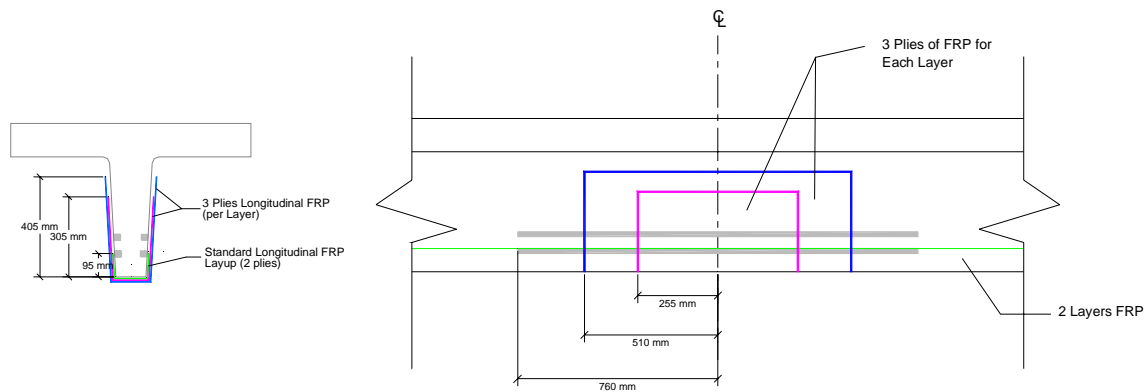
FIGURE 6.12: CFRP Repair Layout for Specimen 5 (Mid-Span)

The CFRP repair was performed in three steps. The first step was the flexural reinforcement used in Specimens 2-4. The next step was place on top of this and wrapped up 305 mm (12 in) on either side of the web. This was composed of three plies of material 510 mm (20 in) long with all fibers oriented with the longitudinal axis of the specimen. At the ends two plies of 200 mm (8 in) wide transverse U-stirrups were applied to provide anchorage to the concrete. On top of this, the third step of CFRP was applied. This consisted of three 1020 mm (40 in) plies that wrapped 410 mm (16 in) up the sides of the web. Once again, all fibers were oriented parallel to the longitudinal axis of the specimen. Two layers of U-Stirrups similar to those above were also applied to the ends of these plies. The repair layout can be seen in Figure 6.12. The

model predicted the stress range within this area would be reduced to 116 MPa (16.8 ksi) from the 262 MPa (38 ksi) seen in Specimen 4.

6.2.2.2 Strain Gage Instrumentation of Specimen 5

Specimen 5 was more heavily instrumented than any of the previous four specimens. Overall, twenty-two gages were put on the specimen with most of them being located in the heavily reinforced midsection. Use of these gages helped to correlate experimental moment-curvature and strain data with that predicted by the analytical model. Included in these gages were gages placed directly on the NSM Rebar. All gages and gage information can be seen in the Table 6.2 and Figure 6.13.

East Elevation

West Elevation
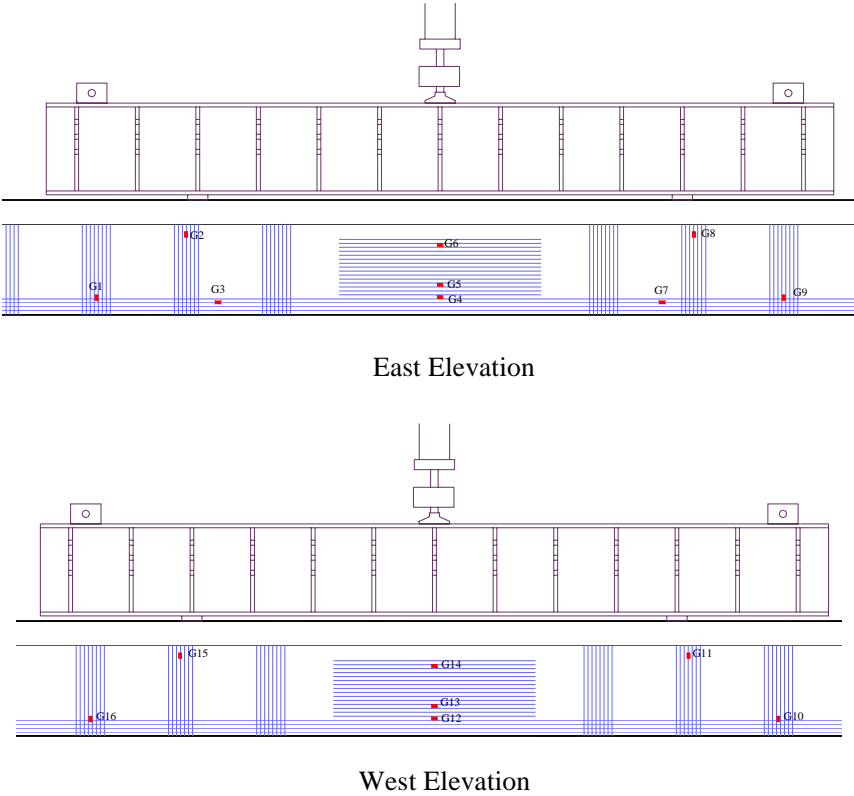
FIGURE 6.13: Gage Locations on Specimen 5

TABLE 6.2: Gages Used for Specimen 5

Gage	Face	Longitudinal Distance From Center (in)	Side of Midspan (N/S)	Vertical Distance From Bottom (in)	Gage Orientation (L/T)*	Gage Description
G1	East	68	S	3.5	T	E68S-3.5T
G2	East	50	S	16	T	E50S-16T
G3	East	44	S	2	L	E44S-2L
G4	East	0	-	3.5	L	E0-3.5L
G5	East	0	-	6	L	E0-6L
G6	East	0	-	14	L	E0-14L
G7	East	44	N	2	L	E44N-2L
G8	East	50	N	16	T	E50N-16T
G9	East	68	N	3.5	T	E68N-3.5T
G10	West	68	S	3.5	T	W68S-3.5T
G11	West	50	S	16	T	W50S-16T
G12	West	0	-	3.5	L	W0-3.5L
G13	West	0	-	6	L	W0-6L
G14	West	0	-	14	L	W0-14L
G15	West	50	N	16	T	W50N-16T
G16	West	68	N	3.5	T	W68N-3.5T
G17	Top	44	S	23	L	T44S-23L
G18	Top	0	-	23	L	T0-23L
G19	Top	44	N	23	L	T44N-23L
G20	Bot	0	-	0	L	B0-0L
G21	Rebar (E)	0	-	3.5	L	R0-3.5L
G22	Rebar (E)	0	-	6	L	R0-6L

* L = Longitudinal; T = Transverse

6.2.2.3 Detailed Results of Specimen 5

Specimen 5 failed after 148,425 load cycles. It failed during the startup procedure immediately after a static reading was taken. The specimen failed underneath the south loading point. Upon further investigation, the strand at this location was badly rusted. The failure location initiated at one of the repaired spall areas where strand had been exposed to the environment. Many of the strands showed signs of very brittle failures that may be attributed to the corrosion. The load-deflection data for the static readings can be seen in Figure 6.14.
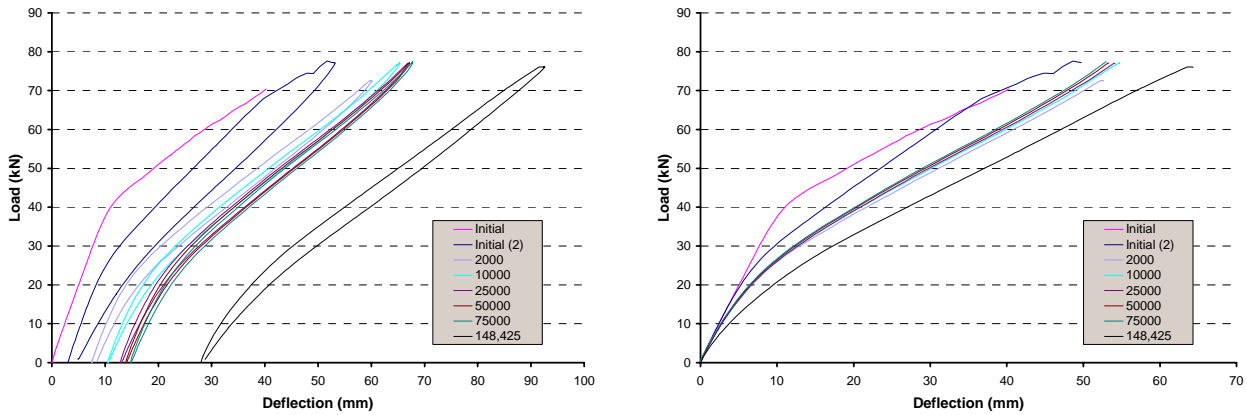
FIGURE 6.14: (a) Load-Deflection Cycles of Specimen 5 (b) Loading Cycles with Common Origin

The data from the static load-deflection reading suggest that Specimen 5 initially underwent a rapid degrading of stiffness. After about 10,000 cycles however, the structure stabilized and stiffness did not change significantly. A large decrease in stiffness as well as significant creep was seen in the final reading. This indicates that overall, the CFRP repair worked very well, and most likely prolonged the life of the specimen. However the strand could not overcome the combination of high stress range and corrosion outside the region protected by additional CFRP sheets and NSM steel bars. Ultimately this is what caused the structure to fail.

Once again, the analytical model was used to predict the experimental load deflection curve and also correlate moment curvature and strain information. The comparison of the initial load-deflection with the experimental data can be seen in Figure 6.15. This figure shows that there is good overall correlation between the curves even though the analysis under predicted the cracking load.
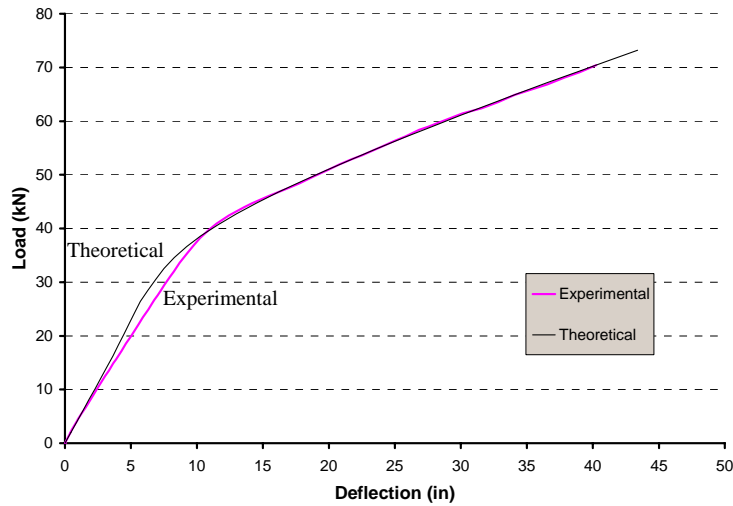
FIGURE 6.15: Comparison of Experimental and Analytical Data for Specimen 5

Good correlation was also found by comparing theoretical and experimental strain behavior at mid-span as shown in Figure 6.16. This figure shows the longitudinal strains at various heights at mid-span at a load of 72 kN (16 kips). It shows data taken from two different static readings, the initial (0 cycles) and final (148,425 cycles) compared with the theoretical strain linear strain distribution at this load level. The analytical model predicted the average curvature well even though it over-predicted the compressive strains and under-predicted the tensile strains. More importantly, there was no significant difference between the strain behavior at initial and that at final. This would indicate the repair at mid-span was remaining stable and was not undergoing any additional deformation due to fatigue factors. It also implies that the stress range in the prestress steel at the initial loading was not changed much during the fatigue process.
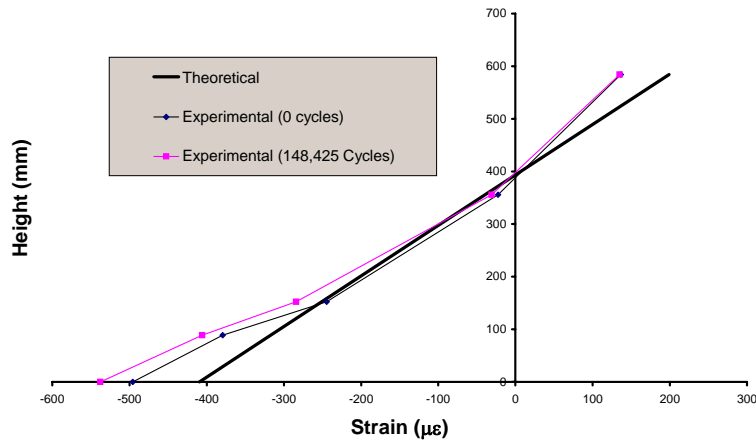
FIGURE 6.16: Strain Data at Mid-Wpan for Specimen 5

6.3   Results of Shear Tests [With Overhang (OH)]

As predicted, it required more load to fail the OH specimens in shear than it did to fail the NOH specimens. The failure load of Specimen 1-OH (the control specimen) was 360 kN (81 kips), nearly 65% more than Specimen 1-NOH and 8% greater than the calculated failure load of 335 kN (75 kips). Specimen 2-OH showed minimal strengthening to 390 kN (87 kips). The increase may be attributed to the longitudinal CFRP wrap holding the web shear cracks closed. Holding the cracks together at a higher load would increase the shear contribution due to aggregate interlock. However, the observed increase is still within the range of typical scatter for shear tests. Load deflection of all four OH specimens can be seen in Figure 6.17.
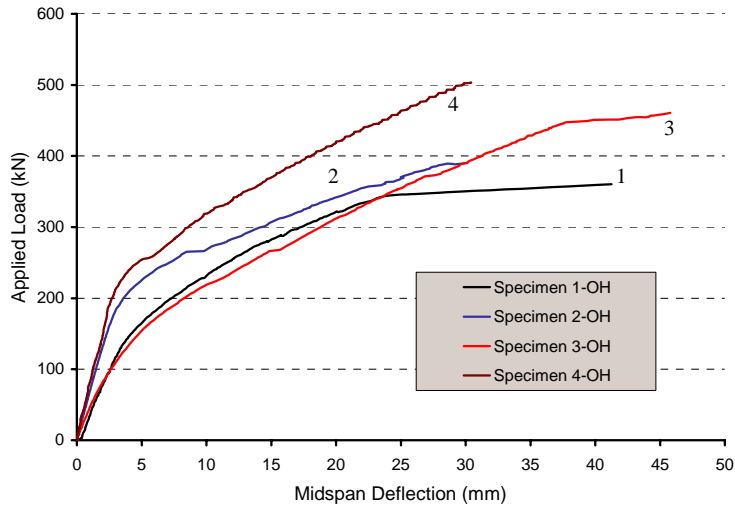
FIGURE 6.17: Load Deflection Data from OH Specimens

A much more substantial increase in shear capacity was seen for Specimen 3-OH and Specimen 4-OH. The CFRP stirrups allowed the failure load for Specimen 3-OH to increase to 465 kN (104 kips), an increase of nearly 28% above the unstrengthened Specimen 1-OH and 22% above the theoretical load of 380 kN (85 kips). This load was high enough to induce a simultaneous flexure-shear failure in the specimen on the side of the loading point towards mid-span. Specimen 4-OH also showed a substantial increase in shear capacity as it failed at an ultimate load of over 503 kN (113 kips). This was a 40% increase in shear capacity compared to the base specimen and 33% greater than the theoretical capacity. Table 6.3 shows a comparison of the performance of the four specimens.

TABLE 6.3 Comparison of Experimental to Theoretical Load Capacity for OH Specimens

	Theoretical Failure Load kN (kip)	Failure Load kN (kip)	% Strengthened from Specimen 1-OH	% Strengthened from Theoretical
Specimen 1-OH	335 (75)	360 (81)	0%	8.0%
Specimen 2-OH	335 (75)	390 (87)	7.4%	16.0%
Specimen 3-OH	380 (85)	465 (104)	28.4%	22.4%
Specimen 4-OH	380 (85)	503 (113)	39.5%	32.9%

6.4   Results of Shear Tests [With No Overhang (NOH)]

In all, five specimens were tested with no overhang. The NOH test for Specimen 2 could not be

performed because the flexural failure destroyed too much of the specimen. Both ends of

Specimen 5 were tested with no overhang. Modifications were also made to the shear layout of

Specimen 5 as well as the test setup. These modifications as well as the test results will be

outlined in the following sections.

6.4.1   *NOH Tests on Specimens 1, 3, and 4*

As predicted, the load to failure for the NOH specimens was considerably less than that

for the respective OH specimens. This was because of the bond-slip failure mode seen in all of

the NOH specimens. A marginal increase in capacity over the base (Specimen 1-NOH) was seen

in Specimens 3-NOH and 4-NOH because of the added shear reinforcement at the ends. The

FRP U-stirrups appeared to hold the primary cracks closed. However, new cracks formed

between the anchoring stirrup and the end. When these cracks propagated into the transfer zone

of the strand, failure occurred immediately. The load-deflection behavior of these three

specimens can be seen in Figure 6.18.

6.4.2   *NOH Tests on Specimen 5*

The flexural failure of Specimen 5 was such that a 4.88 m (16 ft) span could not be used for the

shear tests. Therefore, the span for the shear tests for Specimen 5 was reduced to 4.27 m (14 ft)

with the load point 1.07 m (3.5 ft) from the undamaged end. The FRP reinforcement was also

modified to investigate if the strand-slip failure could be prevented. Instead of using two layers at

305 mm (12 in) wide for the anchor stirrup, a 1220 mm (48 in) wide continuous anchor stirrup

was used. In one test, the anchor stirrup was composed of one layer while in the other test it was

composed of two layers.   The layout for the stirrup can be seen in Figure 6.19. The theory

behind the continuous stirrup was that it would be able to provide a component of force perpendicular to the crack orientation. This could delay or even eliminate the bond-slip failure mode in the prestress.
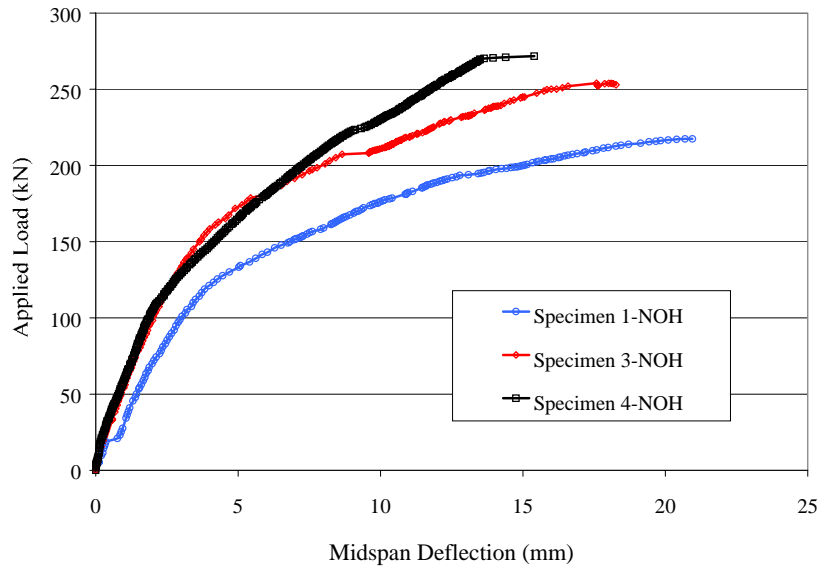
FIGURE 6.18: Load-Deflection Data for NOH Specimens 1 to 4
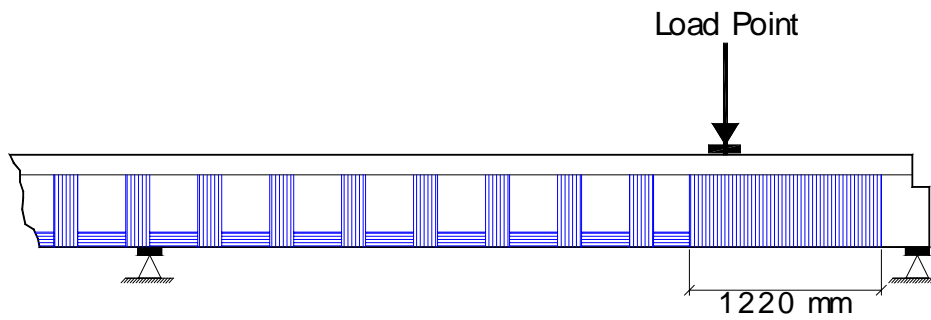
FIGURE 6.19: Shear (NOH) Setup for Specimen 5

The results of the NOH tests on Specimen 5 were very good. Both specimens failed at an ultimate load of approximately 345 kN (75 kips) as seen in Figure 6.20. The end wrapped with two layers showed a greater initial stiffness. However, after cracking the stiffness was identical.

The failure for the end with one layer occurred when the FRP began peeling from the beam. Once this occurred, the cracks underneath immediately propagated to the level of the strand and bond-slip failure ensued. The failure for the end with two layers was similar to this. However, the cracks that caused the failure began forming in the unprotected area between the CFRP and the bearing. These cracks eventually peeled the FRP from the concrete and immediately spread into the transfer zone of the prestress strand causing a bond-slip failure.
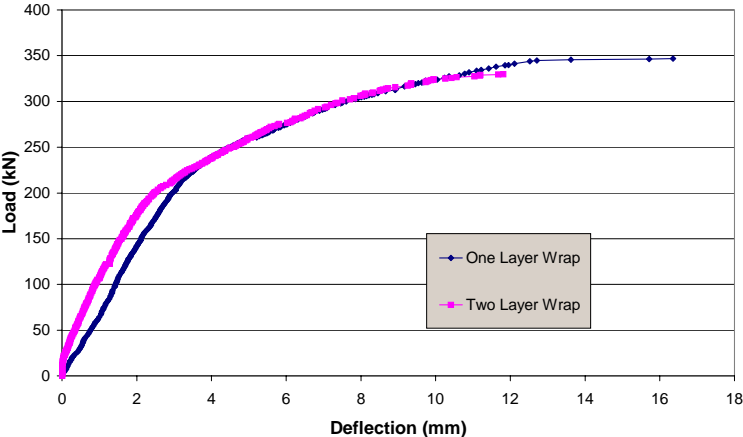
FIGURE 6.20: Load-Deflection Behavior for Specimen 5 (NOH)

Although the repair did not prevent the bond-slip failure, it can still be considered a success because of the increase in shear capacity before the bond-slip failure was initiated. The average shear capacity of the two NOH specimens repaired with the continuous wraps was 40% higher than the shear capacity of the NOH specimens tested with the other anchor detail and 55% greater than the base NOH specimen. A comparison of the shear capacities of the five NOH specimens can be seen in Table 6.4.

TABLE 6.4 Comparison of NOH Shear Specimens

	Failure Load kN (kips)	Shear Capacity kN (kips)	% Strengthened from Specimen 1
Specimen 1-NOH	217 (49)	290 (65)	---
Specimen 3-NOH	253 (57)	337 (76)	16.2%
Specimen 4-NOH	272 (61)	363 (81)	25.2%
Specimen 5-NOH-1 Layer	347 (78)	463 (104)	59.7%
Specimen 5-NOH-2 Layers	329 (74)	439 (99)	51.4%

Chapter 7

Conclusions and Recommendations

7.1   Conclusions

Based on the data gathered from this experimental and analytical study the following conclusions

can be drawn:

- Ultimate flexural strengthening of the damaged beams was accomplished in the static tests. The ultimate capacity of these specimens was increased by over 20% of the actual strength of the base specimen, which corresponds to over 45% of the original design capacity. This increase was accompanied by an increase in stiffness, but the increase in stiffness was relatively small when compared to the increase in ultimate flexural capacity. The small increase in stiffness was because of the small contribution of the CFRP to the overall gross transformed moment of inertia of the beam.

- FRP U-stirrups designed based on a shear friction approach proved successful in overcoming horizontal shear failures. The fact that Specimen 3 failed in FRP rupture rather than horizontal shear indicates that the design was a success.

- The fatigue life of the repaired specimens under the simulated effect of a repeated HS-20 live load ranged between 150,000 to 270,000 cycles. The stress range experienced by the prestress strand at the failure point limited this. In the case of Specimen 5, the failure was also facilitated by strand corrosion at a pre-existing spall.

- If enough reinforcement is provided, the stress range in the prestress strand can be reduced as was evidenced by Specimen 5. The combination of NSM rods and additional CFRP appears to have lowered the stress range at mid-span by over 50%.

- Flexural analysis based on strain compatibility and moment curvature appears to correlate well with experimental data. It also proved to be a good design tool for

both the U-Stirrups as well as the additional reinforcement provided for Specimen 5.

- The CFRP U-Stirrups made shear strengthening of the OH specimens possible. The specimens were strengthened by as much as 30-40%.

- Continuous transverse U-wraps at the ends of the specimens greatly improved the performance of the NOH specimens. Shear capacity was increased by as much as 50% in these specimens. Even with this increase, bond-slip failures could not be avoided. No appreciable gain in performance was noted in the NOH specimens with the standard U-wrap anchors.

7.2   Recommendations

Based on the experimental data and results the following recommendations are made:

- Before any repair or strengthening is made, it is important to first know all details about the beams or girders to be repaired. This includes depth, type, and amount of all flexural reinforcement, areas of corrosion, and amount and type of shear reinforcement. By strengthening a beam without this knowledge, the structure may perform in an undesirable fashion.

- FRP U-stirrups are recommended when flexural strengthening is accomplished. Not only do the U-stirrups provide additional shear reinforcement to the beam, but they also provide additional anchorage of the flexural reinforcement to the concrete surface.

- The methods used for surface preparation of these specimens appear to be adequate. No major areas of debonding were noted during the tests. It is recommended that these methods be used in future strengthening projects.

7.3   Implementation

Based on the research conducted, conclusions withdrawn, recommendations posed and specifications prepared in this report, the CFRP strengthening technique should be readily available for design and implementation to KDOT rural bridge girders, which are showing signs of damage and deterioration but are not scheduled for replacement in the near future.

Chapter 5 and Appendix B of the report provide detailed calculation coverage of the strengthening analysis and design aspects of the application. Chapter 5, coupled with the analysis program developed in this study, serve as an efficient and user-friendly design tool. Section 4.2 and Appendix C present a comprehensive description of the repair of existing damage as well as flexural and shear strengthening to upgrade stiffness and strength. Section 4.2 could serve as concise specifications for KDOT construction and maintenance documents. Chapters 6 and 7 offer KDOT bridge design engineers some guidance on the static and fatigue performance of field-type prototype specimens strengthened in flexure and shear. Appendix D and E may also be used by KDOT materials and research as a guide on material characterization of FRP coupons.

The analysis program developed under this project phase is intended to serve as an effective tool to perform CFRP and NSM strengthening designs. The program is developed as a group of interrelated Excel spread sheets. The first four sheets constitute the input interface. The section geometry and dimensions are entered into the **Section** sheet, which is programmed to handle rectangular and tapered T-sections, Figure 7.1.
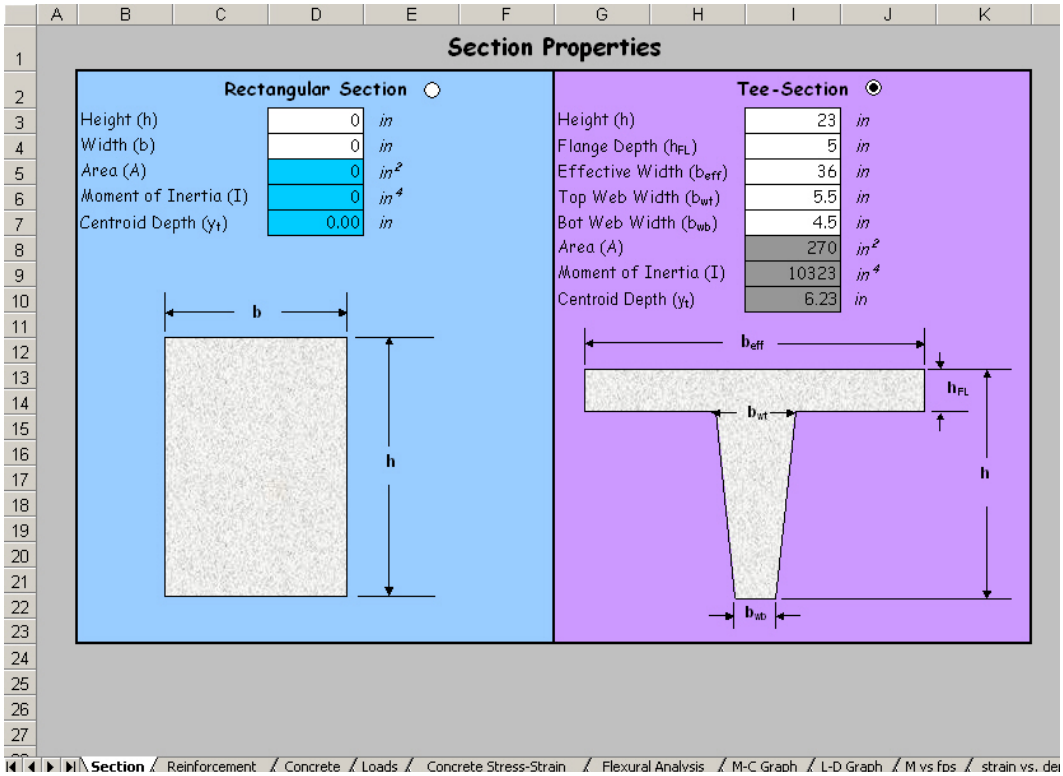
Figure 7.1: Section Input Interface of the Analysis

The reinforcement details are logged into the **Reinforcement** sheet, which is prepared to account for the prestressing strands, mild steel, NSM FRP bars and external FRP sheets, Fig. 7.2.

The properties of the concrete material are entered onto the **Concrete** sheet. These properties include concrete compressive strength, tensile strength, Young's modulus, cracking strain, tension-stiffening parameter and the tensile residual strain at strengthening, Fig. 7.3. This sheet also reports all the transformed section properties and plots the cross section centroid location to-scale.

Figure 7.2: Reinforcement input interface of the analysis

Reinforcement Properties						Material Properties			
Prestress	Strand Size	Number	Area	Depth		f_{pu}	270		ksi
Layer 1	1/2	4	0.612	21		E_{ps}	28,500		ksi
Layer 2	No Strand		0			f_{pi}	162		ksi
Layer 3	No Strand		0			f_{se}	145		ksi
Layer 4	No Strand		0			ε_{ult}	1		in/in
Mild Steel	Bar Size	Number	Area	Depth					
Layer 1	#3	2	0.22	1.5		E_{steel}	29,000		ksi
Layer 2	#3	3	0.33	3.5		f_y	40		ksi
Layer 3	None		0			ε_{ult}	0.05		in/in
Layer 4	None		0						
Glass Bars	Area	Depth							
Layer 1						E_{glass}			ksi
Layer 2						ε_{ult}	0.02		in/in
Layer 3									
Layer 4									
FRP	Width	No. Plies	Area	Depth					
Layer 1	4.5	2	0.0585	23		E_{FRP}	33,000		ksi
Layer 2	1	4	0.026	22.5		ε_{ult}	0.014		in/in
Layer 3	1	4	0.026	21.5		Layer Thickness	0.0065		in
Layer 4	1	4	0.026	20.5		Total Area	0.156		in^2
Layer 5	0.75	4	0.0195	19.625					

P_i 99.14 kips
P_e 88.74 kips

Figure 7.3: Concrete Properties Input Interface of the Analysis

Concrete Material Properties

f'_c	6500	psi
f'_{ci}	3500	psi
f_R	605	psi
ε_{cmax}	0.003	in/in
ε_{tmax}	0.004	in/in
ε_0	0.002	in/in
Ec	6500	ksi

Transformed Section

n_{ps}	4.38	
n_{steel}	4.46	
n_{glass}	0.00	
n_{FRP}	5.08	
Atr	274.8	in^2
Itr	10990	in^4
yttr	6.37	in
ybtr	16.63	in
Sttr	1727	in^3
Sbtr	661	in^3

☑ Tension Stiffening
☑ Precracked
Crack Height 18 in

The **Loads** sheet provides the interface to select the loading scheme used to analyze a simple beam. The sheet has three loading scheme templates for three-point bending, four-point bending and uniform loading, respectively, Figure 7.4. Regardless of the scheme selected, the program automatically includes the effect of uniform self-weight of the beam on the ultimate load-deflection calculation.
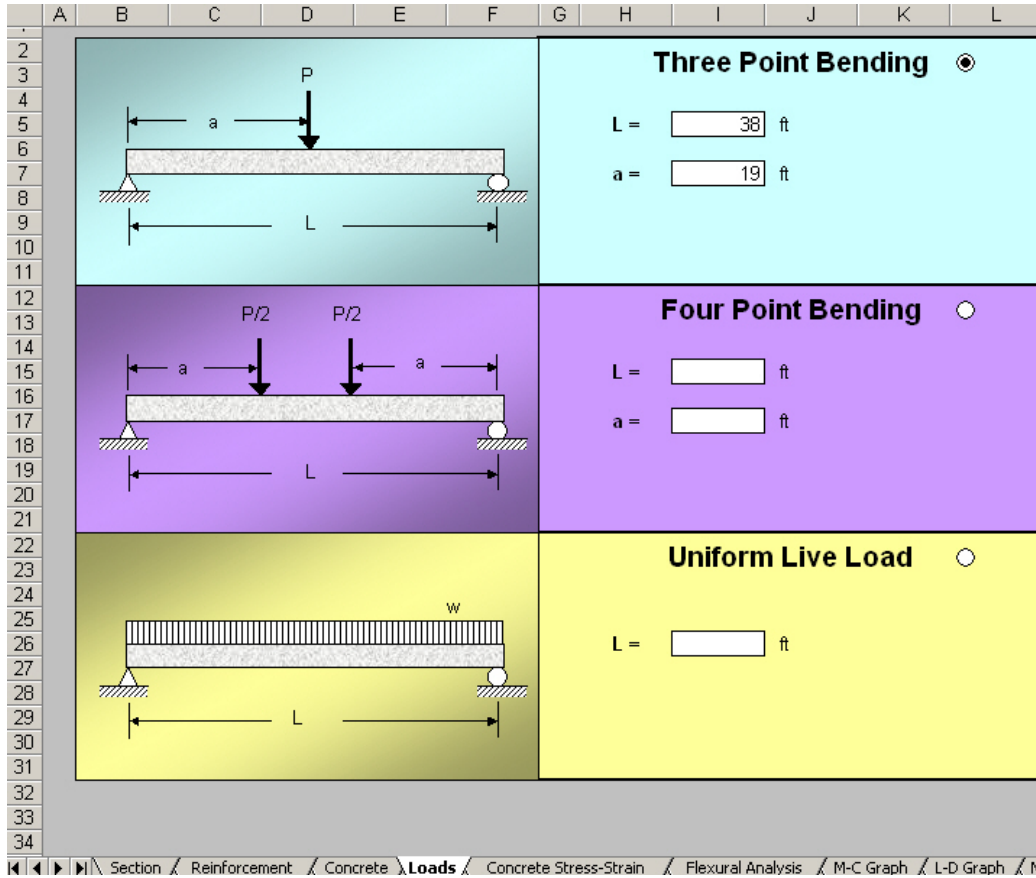
Figure 7.4: Loads Input Interface of the Analysis

The results of the sectional analysis are presented on the **Flexural Analysis** sheet. The sheet has two buttons to compute the moment-curvature and load-deflection response, respectively, Figure. 7.5. Upon completing the section analysis run, the balance of forces, cracking moment, ultimate moment and factored ultimate moment are displayed. Details of

66

strains, stresses, forces and moments generated in each layer of internal and external

reinforcement at ultimate capacity are also tabulated on this sheet. Graphs of the results are

plotted on separate sheets. Moment-curvature response is presented on a sheet called M-C Graph

and load-deflection curve is generated on another sheet named L-D Graph, Fig. 7.5. The

variation in the average prestressing strand stress vs. the applied moment is also plotted

independently on a sheet called "M vs. fps", Fig. 7.5.

	B	C	D	E	F	G	H	I	J	K
Prestress		d	ε	ε_1	ε_2	ε_3	ε_{Total}	f_{ps}	T	M_n
3	Layer 1	21.0	14.63	0.0051	0.00033	0.01286	0.01828	266	163.1	275
4	Layer 2	0	0	0	0	0	-0.0015	-42	0	0
5	Layer 3	0	0	0	0	0	-0.0015	-42	0	0
6	Layer 4	0	0	0	0	0	-0.0015	-42	0	0

	B	C	D	E	F	G
Mild Steel		d	ε	f_s	T	M_n
9	Layer 1	1.5	-0.00046	-13.3	-2.92	-0.17
10	Layer 2	3.5	0.00091	26.3	8.69	1.97
11	Layer 3	0	0	0	0	0
12	Layer 4	0	0	0	0	0

	B	C	D	E	F	G
FRP Bars		d	ε	f_{glass}	T	M_n
15	Layer 1	0	0	0	0	0
16	Layer 2	0	0	0	0	0
17	Layer 3	0	0	0	0	0
18	Layer 4	0	0	0	0	0

	B	C	D	E	F	G	H
FRP Wraps		d	ε_b	ε	f_{FRP}	T	M_n	$0.85*M_n$
21	Layer 1	23	-0.00021	0.01401	462	27.1	50	43
22	Layer 2	22.5	-0.00022	0.01367	451	11.7	21	18
23	Layer 3	21.5	-0.00021	0.01299	429	11.1	19	16
24	Layer 4	20.5	-0.00020	0.01232	407	10.6	17	15
25	Layer 5	19.625	-0.00019	0.01173	387	7.5	12	10

Reinforcement Tension 236.9 *kips*
Concrete Tension 46.5 *kips*
Concrete Compression -283.4 *kips*
Total 0.0 *kips*

GoalSeek

Failure Mode   FRP Rupture   M - φ
100% Complete   P - Δ

Mcr 159.3 *k-ft*
Mn 406.8 *k-ft*
φMn 388.8 *k-ft*

Section / Reinforcement / Concrete / Loads / Concrete Stress-Strain / **Flexural Analysis** / M-C Graph / L-D Graph / M vs fps / strain vs. depth / M

FIGURE 7.5: Flexural Analysis Output Module of the Program

67

NOTATIONS

A_c	=	Gross area of concrete section
A_{FRPi}	=	Area of FRP in FRP layer i
A_{pi}	=	Area of prestress steel in prestress layer i
A_p	=	Total area of prestressing steel
A_{si}	=	Area of steel in steel layer i
A_{fv}	=	Total area of one strip of transverse FRP reinforcement = 2n t_f w_f (in^2)
A_{vf}	=	Area of transverse FRP reinforcement per unit length = A_{fv}/S_f
b_{ci}	=	width of concrete layer i
b_w	=	width of section web
c	=	depth of neutral axis
d_{ci}	=	depth to concrete layer i
d_f	=	depth to the FRP shear reinforcement
d_{FRPi}	=	depth to FRP layer i
d_{pi}	=	depth to prestress layer i
d	=	depth to the centroid of tension reinforcement (prestressed and/or mild)
d_{si}	=	depth to steel layer i
e_{avg}	=	average eccentricity of all prestressed layers
e_{pi}	=	eccentricity of prestress layer i
E_c	=	Young's Modulus of concrete
E_{FRP}	=	Young's Modulus of FRP
E_p	=	Young's Modulus of prestressing steel
E_s	=	Young's Modulus of reinforcing steel
f'_c	=	Concrete strength of standard cylinders
f_{ci}	=	Stress in concrete layer i
f_F	=	Allowable tensile stress in transverse FRP (100MPa, 690 ksi)
f_{fe}	=	Stress level in the FRP shear reinforcement at failure
f_{FRPi}	=	Stress in FRP layer i
f_{pi}	=	Stress in prestress layer i
f_R	=	Modulus of rupture of concrete
f_{si}	=	Stress in steel layer i
f_y	=	Yield Stress of Steel
F_{ci}	=	Force in concrete layer i
F_{FRPi}	=	Force in FRP layer i
F_{pi}	=	Force in prestressing steel layer i
F_{si}	=	Force in steel layer i
I_c	=	Gross moment of inertia of concrete section
M_{Load}	=	Moment caused by the load on the beam at time of FRP placement
P_{se}	=	Prestressing force after losses
P_e	=	Prestressing force after losses
S_f	=	Spacing of FRP external shear reinforcement
V_c	=	Concrete shear strength
V_f	=	Shear strength of FRP external transverse U wraps
V_n	=	Nominal shear strength

V_p	=	Prestress shear strength
V_s	=	Steel stirrup shear strength
$\varepsilon_{c/FRP}$	=	Strain in concrete at the level of external reinforcement
ε_{ci}	=	Stress in concrete layer i
ε_{cr}	=	Cracking strain of concrete
$\varepsilon_{initial}$	=	Concrete strain at the FRP level during FRP strengthening
ε_{FRPi}	=	Stress in FRP layer i
ε_{pi}	=	Stress in prestress layer i
ε_{si}	=	Stress in steel layer i
ε_o	=	Strain corresponding to f'_c
ε_1	=	Strain in prestressing strand due to its tension force after losses
ε_2	=	Strain in concrete fiber adjacent to strand due to prestressing
ε_3	=	Tensile strain in strand due to loading
ϕ	=	Section curvature
μ	=	Friction coefficient of the ACI shear friction model

REFERENCES

AASHTO (1996). *Standard Specifications for Highway Bridges* (Sixteenth Edition). American Association of State Highway Transportation Officials, Washington D.C.

ACI Committee 318 (1999), *Building Code Requirements for Structural Concrete (ACI 318-99) and Commentary (ACI 318R-99)*. American Concrete Institute, Farmington Mills, MI.

Alkhradaji, T., Nanni, A., Mayo, R. (2000). "Upgrading Missouri Transportation Infrastructure: Solid Reinforced-Concrete decks strengthened with Fiber-Reinforced Polymer Systems." *Transportation Research Record no. 1740*. National Academy Press, Washington D.C., 157-163.

Arduini, M. and Nanni, A. (1997a). "Behavior of Pre-cracked RC Beams Strengthened with carbon CFRP Sheets." *Journal of Composites for Construction,* May, 63-70.

Arduini, M. and Nanni, A. (1997b). "Parametric Study of Beams with Externally Bonded FRP Reinforcement." *ACI Structural Journal.* Sep-Oct, 493-501.

Dussek, I. J. (1980). "Strengthening of Bridge Beams and Similar Structures by Means of Epoxy-Resin-Bonded External Reinforcement." *Transportation Research Record No. 785*, Transportation Research Board, Washington, D.C., 21-24.

El-Tawil, Sherif, Ogunc, C., Okeil, A., and Shahawy, M. (2001). "Static and Fatigue Analyses of RC Beams Strengthened with CFRP Laminates," *Journal of Composites for Construction, November*, 258-267.

Fanning J. Paul and Kelly, Oliver (2001). "Ultimate Response of RC Beams Strengthened with CFRP Plates," *Journal of Composites for Construction*, May 122-127.

Federal Highway Administration (2001). "FHWA National Bridge Inventory (NBI)," *www.fhwa.dot.gov/bridge/nbi.htm*

Meier, U. and Kaiser, H. (1991) "Strengthening of Structures with CFRP Laminates: In Advanced Composite Materials in Civil Engineering Structures*," Proceedings of the Specialty Conference*, Las Vegas, NV, January 31-February 1, ASCE, New York, pp. 288-301.

Meier, U., Deuring, M., Meier, H., and Schweger, G. (1992), "Strengthening of Structures with CFRP Laminates: Research and Applications in Switzerland", *Proceedings of the First International Conference On Advanced Composite Materials In Bridges And Structures*, Sherbrooke, Que., October, pp. 243-251.

M-Brace (1998). *M-Brace Composite Strengthening System-Engineering Design Guidelines* (Second Edition) Master Builders Technologies, Cleveland, OH.

Nanni, A. (1995). "Concrete Repair with Externally Bonded CFRP Reinforcement: Examples from Japan." *ACI Concrete International,* June, 22-26.

Nilson, A. H. (1987), *Design of Prestressed Concrete,* (Second edition) John Wiley and Sons Inc., New York, NY.

Norris, T., Saadatmanesh, H., Ehsani, M. (1997). "Shear and Flexural Strengthening of RC Beams with Carbon Fiber Sheets," *Journal of Structural Engineering*, July, 903-911.

Park, R., and Paulay, T. (1975). *Reinforced Concrete Structures*, John Wiley and Sons, Inc., New York, N.Y.

Precast/Prestress Concrete Institute (1999). *PCI Design Handbook*, 5th Edition, Chicago, Illinois.

Quantrill, R. J., Hollaway L. C. and Thorne, A. M. (1996). " Experimental and Analytical Investigation of FRP Strengthened Beam Response: Part I," *Magazine of Concrete Research*, 1996, 48, No. 177, pp 331-342.

Ritchie, P. A., Thomas, D. A., Lu, L.-W. and Connelly, G. M., (1991) "External Reinforcement of Concrete Beams Using Fiber Reinforced Plastics", *ACI Structural Journal, ACI,* Vol. 88, No. 4, pp. 490-500.

Rizkalla, S. H., and Erki, M. A. (1991) "Advanced Composite Materials with Applications to Bridges: *Edited by* A. A. Mufti, M. A. Erki and L. G. Jaeger: State of the Art Report," *Canadian Society of Civil Engineers*, Montreal, Que., pp. 231-273.

Russell, B. and Burns, N. (1993). "Design Guidelines for Transfer, Development and Debonding of Large Diameter Seven Wire Strands in Pretensioned Concrete Girders," Texas Department of Transportation in cooperation with Federal Highway Administration Research Report 1210-5F, January 1993, 286 pages.

Saadatmanesh, H., and Ehsani, M. R., (1990) " FRP Plates Can Strengthen Beams", *Concrete International, ACI,* Vol. 99, No. 7, pp. 41-47.

Saadatmanesh, H., and Ehsani, M. R., (1991) "RC Beams strengthened with GFRP Plates, I: Experimental Study", *Journal of Structural Engineering, ASCE,* Vol. 117, No. 11, pp. 3417-3433.

Shahawy, M. and Beitelman, T. (1999). "Static and Fatigue Performance of RC beams Strengthened with CFRP Laminates," *Journal of Structural Engineering,* June, 613-621.

Spadea, G., Bencardino F. and Swamy, R. N. (1998), "Structural Behavior of Composite RC Beams with Externally Bonded CFRP", *Journal of Composites for Construction, ASCE,* Vol. 2, No. 3, pp. 132-136.

Triantafillou, T. C., Deskovic, N. and Deuring, M. (1992). "Strengthening of Reinforcing Concrete Structures with Prestressed Fiber Reinforced Plastic Sheets," *ACI Structural Journal,* V. 89, No. 3, pp. 235-244.

Varastehpour, H. and Hamelin, P. (1997), "Strengthening of Concrete Beams using Fiber Reinforced Plastic", *Materials and Structures/ Matériaux et Constructions*, Vol. 30, April 1997, pp 160-166.

Wang, Y. C. and Restrepo, J. I. (2001). "Response of T-Beams Strengthened for Flexure with Staggered CFRP Plates," *Journal of Composites for Construction,* August, 188-199.

Appendix A

Crack Maps

Specimen 1: Pre-Existing Cracks

West Elevation

East Elevation

Specimen 2: Pre-Existing Cracks
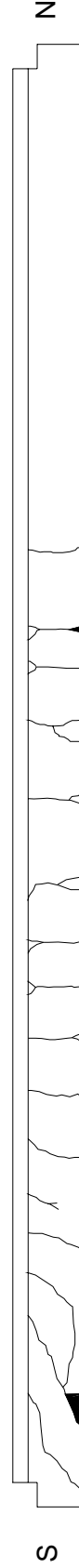
West Elevation

East Elevation

Specimen 3: Pre-Existing Cracks
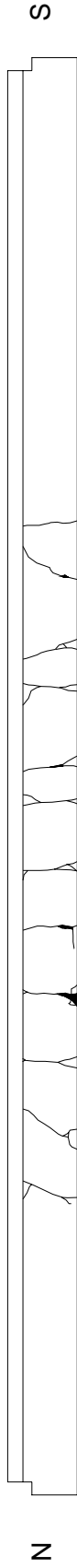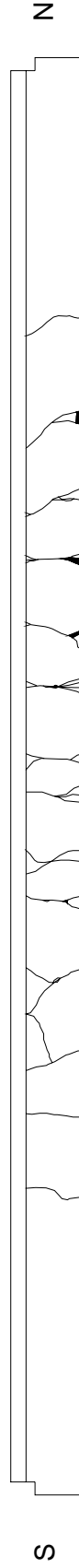
West Elevation

East Elevation

Specimen 4: Pre-Existing Cracks
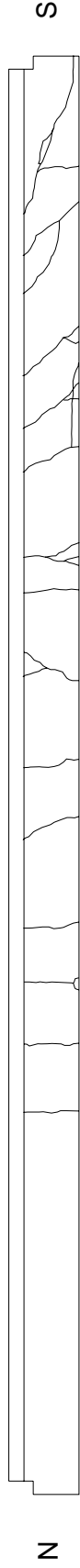
West Elevation

East Elevation

Specimen 5: Pre-Existing Cracks
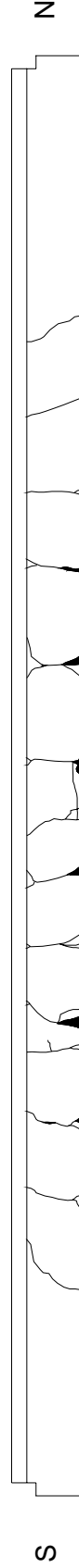
West Elevation

East Elevation

Specimen 1: Cracks at Failure
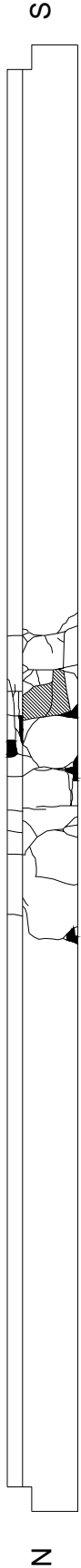
West Elevation

East Elevation

Specimen 2: Cracks at Failure
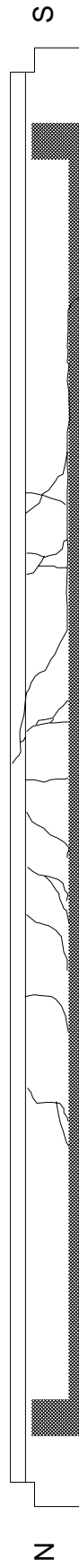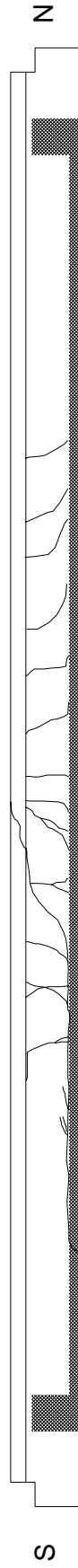
West Elevation

East Elevation

Specimen 3: Cracks at Failure
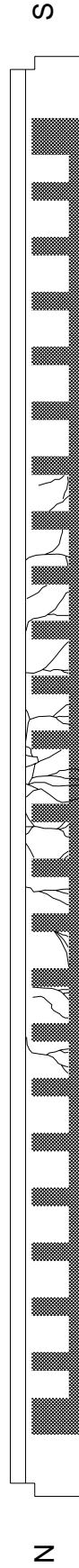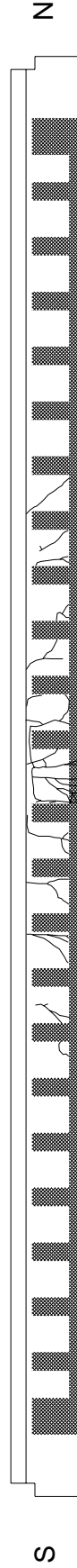
West Elevation

East Elevation

Specimen 4: Cracks at Failure
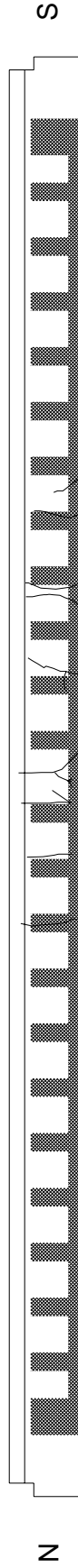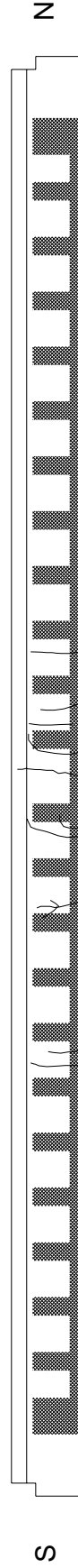
West Elevation

East Elevation

Specimen 5: Cracks at Failure
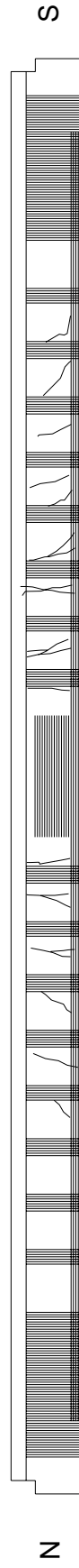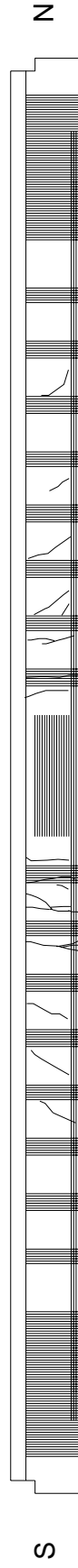
West Elevation

East Elevation

Appendix B

Calculations

Calculated Losses For Prestress Strand (Metric)
From 4.7.3 of PCI Design Handbook

Total Losses:

$$T.L. = ES + CR + SH + RE$$

where,

ES = Losses due to elastic shortening
CR = Losses due to creep
SH = Losses due to shrinkage
RE = Losses due to relaxation

Elastic Shortening:

$$ES = \frac{K_{es} E_{ps} f_{cir}}{E_{ci}}$$

$$f_{cir} = K_{cir}\left[\frac{P_i}{A_g} + \frac{P_i e^2}{I_g}\right] - \frac{M_g e}{I_g}$$

$$f_{cir} = 0.9\left[\frac{516}{174,000} + \frac{516(376)^2}{4.21 \times 10^9}\right] - \frac{68,500(376)}{4.21 \times 10^9} = 12.15 \ \text{MPa}$$

$$ES = \frac{1.0(200)(12.15)}{25} = 97.2 \ \text{MPa}$$

Creep:

$$CR = K_{cr}\frac{E_{ps}}{E_c}\left(f_{cir} - f_{cds}\right)$$

$$f_{cds} = \frac{M_{sd} e}{I_g} = \frac{68,500(376)}{4.21 \times 10^9} = 6.12 \ \text{MPa}$$

$$CR = 2.0\frac{200}{34.5}(12.15 - 6.12) = 69.9 \ \text{MPa}$$

Shrinkage (English):

$$SH = 8.2 \times 10^{-6} K_{sh} E_{ps} \left(1 - \frac{0.06V}{S}\right)(100 - R.H.)$$

$$\frac{V}{S} = \frac{Area}{Perimeter} = \frac{270}{226} = 1.195 \text{ in}$$

$$SH = 8.2 \times 10^{-6}(1.0)(28{,}500)(1 - 0.06(1.195))(100 - 50) = 10.8 \text{ ksi}$$
$$(74.5 \text{ MPa})$$

Relaxation (English):

$$RE = [K_{re} - J(SH + CR + ES)]C$$

$$= [20 - 0.15(35.25)]1.0 = 14.7 \text{ ksi } (101.4 \text{ MPa})$$

Total Losses

$$TL = 97.2 + 69.6 + 74.5 + 101.4 = 342.7 \text{ MPa}$$

Calculated Flexural Strengthening for FRP Phase I Beams (Metric)
From AASHTO Standard Specification (1996)

Combination of Loads (3.22.1)

$$M_u = 1.3[M_D + 1.67(M_L + I)]$$

Dead Load

$$M_D = \frac{w_{self} L^2}{8} = \frac{(4.09)(12.04)^2}{8} = 74.1 \text{ kN-m}$$

Live Load

$$M_L = \frac{M_L^*}{2} \cdot D.F.$$

where,

$$M_L^* = \begin{cases} 347 \text{ kN-m (H-15)} \\ 598 \text{ kN-m (HS-20)} \\ 747 \text{ kN-m (HS-25)} \end{cases}$$

$$D.F. = \frac{S}{6.0} = \frac{0.914(3.281)}{6} = 0.5 \qquad \text{(Table 3.23.3.1)}$$

$$M_L = \begin{cases} 87 \text{ kN-m (H-15)} \\ 149 \text{ kN-m (HS-20)} \\ 187 \text{ kN-m (HS-25)} \end{cases}$$

Impact Factor (3.8.2.1)

$$I = \frac{50}{L+125} \leq 30\%$$

$$I = \frac{50}{12.04(3.281)+125} = 30.4\% \qquad \therefore I = 30\%$$

Moment Capacity with H-15 Design Live Load

$$M_u = 1.3[74.1 + 1.67(1.3(87))] = 341.2 \text{ kN-m}$$

Moment Capacity with HS-20 Design Live Load

$$M_u = 1.3[74.1 + 1.67(1.3(149))] = 517.3 \text{ kN-m}$$

$\quad$% Increase in TOTAL moment capacity = **51.6%**
$\quad$% Increase in LL moment capacity = **71.9%**

Moment Capacity with HS-25 Design Live Load

$$M_u = 1.3[74.1 + 1.67(1.3(187))] = 624.6 \text{ kN-m}$$

$\quad$% Increase in TOTAL moment capacity = **83.0%**
$\quad$% Increase in LL moment capacity = **115.6%**

Design of U-Stirrups for FRP Phase I Beams (Metric)
Design Based on ACI 318-99 Section 11.7.4 (Shear Friction)

The required area of shear-transfer reinforcement is computed by:

$$A_{vf} = \frac{V_u}{\phi f_y \mu} \qquad\qquad (11\text{-}25)$$

where,

$f_y = f_{allow}$ for FRP, 690 MPa
$\mu = 1.4$ for monolithic concrete
$\phi = 0.85$ for shear

<u>Determination of V_u</u>

From flexural analysis program, the maximum tension force developed in the beam at midsection at ultimate load is:

$$V_u = \begin{cases} 1045 \text{ kN (Level 1 Strength)} \\ 1334 \text{ kN (Level 2 Strength)} \end{cases}$$

This force must be developed over the entire half-length of the simply supported beam (5.79 m). Therefore, the shear force per foot of beam is:

$$V_u = \begin{cases} \dfrac{1045}{5.79} = 180.5 \text{ kN/m (Level 1 Strength)} \\[3mm] \dfrac{1334}{5.79} = 230.4 \text{ kN/m (Level 2 Strength)} \end{cases}$$

 <u>Reinforcement Needed</u>
1) *Level 1 Strengthening*

$$A_{vf(req'd)} = \frac{V_u}{\phi f_y \mu} = \frac{180.5}{0.85(690)(1.4)} = 220 \text{ mm}^2/\text{m}$$

Provide two layers of 152 mm wide stirrups at 456 mm center-to-center spacing

$$A_{vf(prov)} = \frac{nwt}{s} = \frac{2(2)(152)(0.165)}{0.456} = 220 \text{ mm}^2/\text{m} \qquad\qquad \text{O.K.}$$

2) *Level 2 Strengthening*

$$A_{vf(req'd)} = \frac{V_u}{\phi f_y \mu} = \frac{230.4}{0.85(690)(1.4)} = 281 \text{ mm}^2/\text{m}$$

Provide three layers of 152 mm wide stirrups at 456 mm center-to-center spacing

$$A_{vf(prov)} = \frac{nwt}{s} = \frac{2(3)(152)(0.165)}{0.456} = 330 \text{ mm}^2/\text{m} \qquad \text{O.K.}$$

where,

n = number of FRP Layers
w = width of FRP U-Stirrup (mm)
t = thickness of FRP sheets (mm)
s = spacing of U-Stirrups (m)

Appendix C

Repair Methods

Epoxy Injection

Installed injection ports

Injection port

Buttering Cracks

Buttering around injection port

Buttered cracks

Buttered cracks and injection ports

FRP Wet Lay-Up

Sand blasting surface

Marking FRP position with duct tape

Applying primer

Applying primer

Applying saturant

Placing first layer

Placing second layer

Repaired Specimen

NSMR Placement

Cutting grooves

Chiseling out grooves

NSMR grooves

Placing rebar in groove

Finished NSM repair

Appendix D

Repair Material Properties

PRO-POXY 300
ASTM C-881
TYPES I, II, IV & V
GRADE 3, CLASSES B & C

LABORATORY TESTS	RESULTS	SPECIFICATIONS	
C-881 Consistency	0 (no flow)		
C-881 Gel Time	35 Minutes	30 Minutes$_{1,2,4,5}$	Minimum
C-882 Bond Strength (2 day cure)	2,232 PSI	1,000 PSI$_{1,4}$	Minimum
C-882 Bond Strength (14 day cure)	2,460 PSI	1,500 PSI$_{1,2,4,5}$	Minimum
D-570 Absorption	0.63%	1.0%$_{1,2,4,5}$	Maximum
D-2566 Linear Coefficient of Shrinkage	0.0007	0.005$_{1,2,4,5}$	Maximum
D-695 Compressive Strength	11,236 PSI	5,000 PSI$_2$ 8,000 PSI$_{1,5}$ 10,000 PSI$_4$	Minimum
D-695 Compressive Modulus	250,100 PSI	90,000 PSI$_2$ 150,000 PSI$_{1,5}$ 200,000 PSI$_4$	Minimum
D-638 % Elongation at Break	2.56%	1.0%$_{1,2,4,5}$	Minimum
D-732 Shear Strength	3,550 PSI	None	
D-790 Flexural Strength	5,582 PSI	None	
C-884 Shrinkage	Pass	None	
C-884 Thermal Compatibility	Pass	None	

$_1$ - ASTM C-881 Type I
$_2$ - ASTM C-881 Type II
$_4$ - ASTM C-881 Type IV
$_5$ - ASTM C-881 Type V

01/17/96

97

PRO-POXY 50
ASTM C-881
TYPES I, II, IV & V
GRADE 1, CLASSES B & C

LABORATORY TESTS	RESULTS	SPECIFICATIONS	
D-2393 Viscosity	175 cps	2000 cps	Maximum
C-881 Gel Time	45 Minutes	30 Minutes[1,2,4,5]	Minimum
C-882 Bond Strength (2 day cure)	2,413 PSI	1,000 PSI[1,4]	Minimum
C-882 Bond Strength (14 day cure)	3,612 PSI	1,500 PSI[1,2,4,5]	Minimum
D-570 Absorption	0.85%	1.0%[1,2,4,5]	Maximum
D-648 Heat Deflection Temperature	50°C	49°C[4,5]	Minimum
D-2566 Linear Coefficient of Shrinkage	0.0021	0.005[1,2,4,5]	Maximum
D-695 Compressive Strength	10,685 PSI	5,000 PSI[2] 8,000 PSI[1,5] 10,000 PSI[4]	Minimum
D-695 Compressive Modulus	210,000 PSI	90,000 PSI[2] 150,000 PSI[1,5] 200,000 PSI[4]	Minimum
D-638 Tensile Strength	7,010 PSI	2,000 PSI[2] 5,000 PSI[1] 6,000 PSI[5] 7,000 PSI[4]	Minimum
D-638 % Elongation at Break	2.96%	1.0%[1,2,4,5]	Minimum
D-732 Shear Strength	9,040 PSI	None	
D-790 Flexural Strength	9,664 PSI	None	
C-881 Filler Content	0.0%	None	
C-883 Shrinkage	Pass	None	
C-884 Thermal Compatibility	Pass	None	

[1] - ASTM C-881 Type I
[2] - ASTM C-881 Type II
[4] - ASTM C-881 Type IV
[5] - ASTM C-881 Type V

04/11/97

98

PRO-POXY TYPE III DOT
ASTM C-881
TYPES III, GRADE 1
CLASSES B & C

LABORATORY TESTS	RESULTS	ASTM C881 SPECIFICATIONS
Resin Properties		
Mix Ratio	1 to 1 by volume	None
D-695 Compressive Modulus	64,820	130,000 maximum
D-638 Tensile Strength	2,610 psi	None
D-638 Tensile Elongation	49%	30% minimum
C-882 Bond Strength (14 day cure)	3,470 PSI	1,500 psi minimum
D-570 Absorption	0.19%	1.0% maximum
C-881 Gel Time	30 Minutes[1]	30 minutes minimum
C-881 Brookfield Visc. RV3 @20rpms	1425 cps	2000 cps maximum
D-2240 Shore D Hardness	69	None
C-883 Shrinkage	Pass	Pass
C-884 Thermal Compatibility	Pass	None
AASHTO T-277 Chloride Ion Permeability	0.9 coulombs	None
Grout Properties (sand to resin / 3.5 to 1 by volume)		
C-579[2] Compressive Strength 3 hrs	1100 psi	N/A
C-579[2] Compressive Strength 24 hrs	7500 psi	N/A
C-579[2] Compressive Strength 48 hrs - Moist Cure	7000 psi	N/A

04/08/98

[1] - Class B
[2] - C-579 Method B with Plastic Inserts

99

MBrace Fiber	Ultimate Strength ksi (MPa)	Design Strength ksi (MPa)	Tensile Modulus ksi (MPa)
CF 130 High Tensile Carbon	620 (4275)	550 (3790)	33,000 (228,000)
CF 530 High Modulus Carbon	584 (4027)	510 (3517)	54,000 (372,000)
EG 900 E-Glass	251 (1730)	220 (1517)	10,500 (72,400)
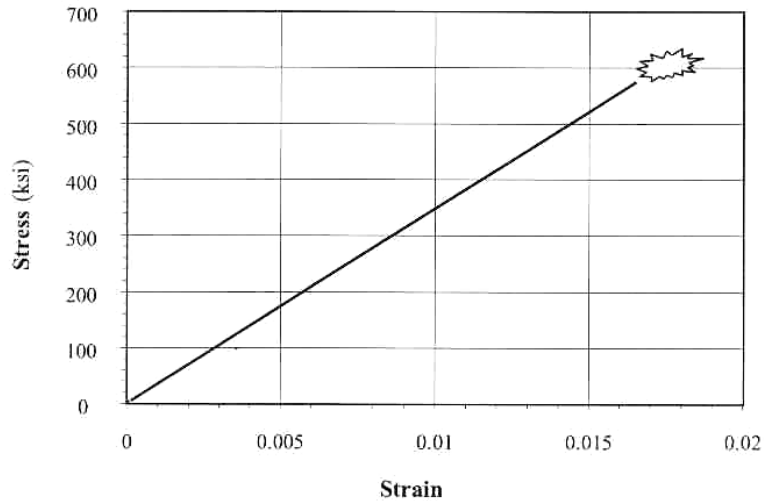
Carbon Fiber Properties *(M-Brace Design Guide, 1998)*

	MBrace Primer	MBrace Putty	MBrace Saturant
Maximum Stress psi (MPa)	2500 (17.2)	2200 (15.2)	8000 (55.2)
Stress at Yield psi (MPa)	2100 (14.5)	1900 (13.1)	7800 (53.8)
Stress at Rupture psi (MPa)	2500 (17.2)	2100 (14.5)	7900 (54.5)
Strain at Max. Stress	0.400	0.060	0.030
Strain at Yield	0.040	0.020	0.025
Strain at Rupture	0.400	0.070	0.035
Elastic Modulus psi (MPa)	104,000 (715)	260,000 (1790)	440,000 (3035)
Poisson's Ratio	0.48	0.48	0.40

Note: Properties determined at 72 °F (20 °C) and 40% relative humidity.

Tensile Properties of Wet-Lay Up Epoxies

100

	MBrace Primer	MBrace Putty	MBrace Saturant
Maximum Stress psi (MPa)	3500 (24.1)	4000 (27.6)	20,000 (138)
Stress at Yield psi (MPa)	3500 (24.1)	3800 (26.2)	20,000 (138)
Stress at Rupture psi (MPa)	Large deformation with no rupture.	3700 (25.5)	18,000 (124)
Strain at Max. Stress	0.060	0.060	0.042
Strain at Yield	0.050	0.040	0.038
Strain at Rupture	Large deformation with no rupture.	0.070	0.050
Flexural Modulus psi (MPa)	86,300 (595)	130,000 (895)	540,000 (3724)

Note: Properties determined at 72 °F (20 °C) and 40% relative humidity.

Flexural Properties of Wet-Lay Up Epoxies

	MBrace Primer	MBrace Putty	MBrace Saturant
Maximum Stress psi (MPa)	4100 (28.3)	3300 (22.8)	12,500 (86.2)
Stress at Yield psi (MPa)	3800 (26.2)	3300 (22.8)	12,500 (86.2)
Strain at Max. Stress	0.100	0.100	0.050
Strain at Yield	0.040	0.050	0.050
Compressive Modulus, psi (MPa)	97,000 (670)	156,000 (1075)	380,000 (2620)

Note: Properties determined at 72 °F (20 °C) and 40% relative humidity.

Compressive Properties of Wet-Lay Up Epoxies

Appendix E

Results of Tensile Tests on CF-130

MB-4

Specimen	E_{comp}	E_{fiber}	f_u (fiber)	Failure Mode
1	7,685	33,580	266	SIV
2	7,049	29,497	394	XVV
3	8,431	34,243	434	SVV
4	8,269	33,584	339	SGT
5	8,191	34,719	446	SGV
Average	**7,925**	**33,125**	**376**	
Std Dev	**563**	**2,084**	**74**	

Longitudinal Fiber Stress vs. Strain for MB-4 Samples
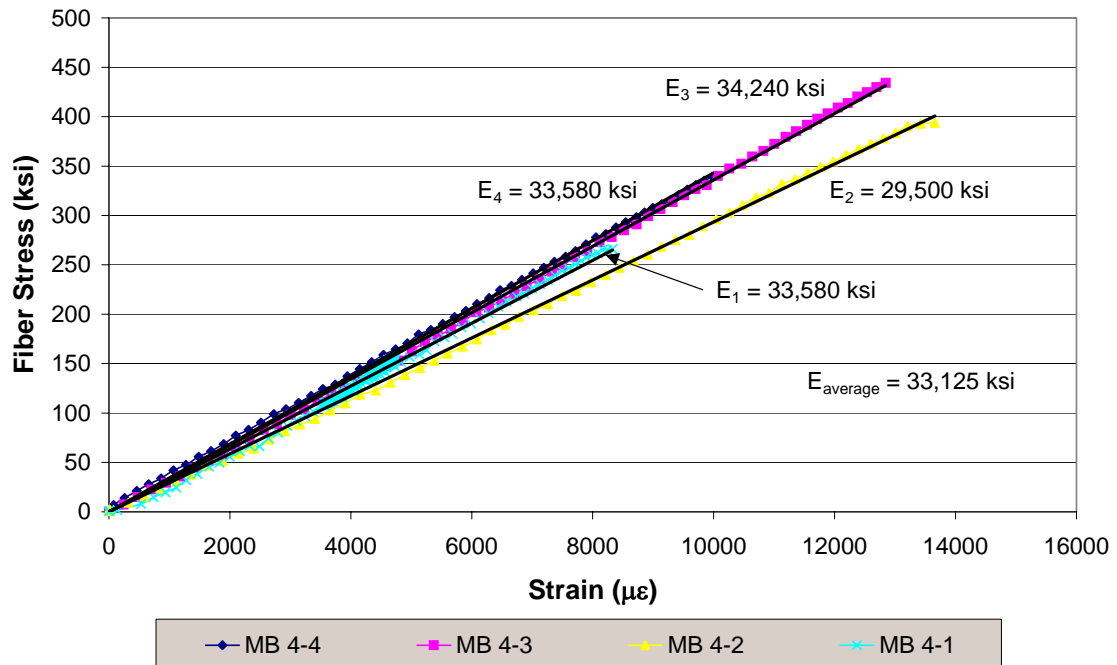
MB-6

Specimen	E_{comp}	E_{fiber}	f_u (fiber)	Failure Mode
1	6,136	30,209	338	SGM
2	6,851	32,657	441	XWT
3	6,848	33,448	467	GAT
4	N / A	N / A	N / A	N / A
5	7,045	34,685	546	XMG
Average	6,720	32,750	448	
Std Dev	400	1,888	86	

Longitudinal Fiber Stress vs. Strain for MB-6 Samples

$E_5 = 34,700$ ksi

$E_3 = 33,400$ ksi

$E_2 = 32,700$ ksi

$E_1 = 30,300$ ksi

$E_{average} = 32,750$ ksi

Fiber Stress (ksi)

Strain ($\mu\varepsilon$)
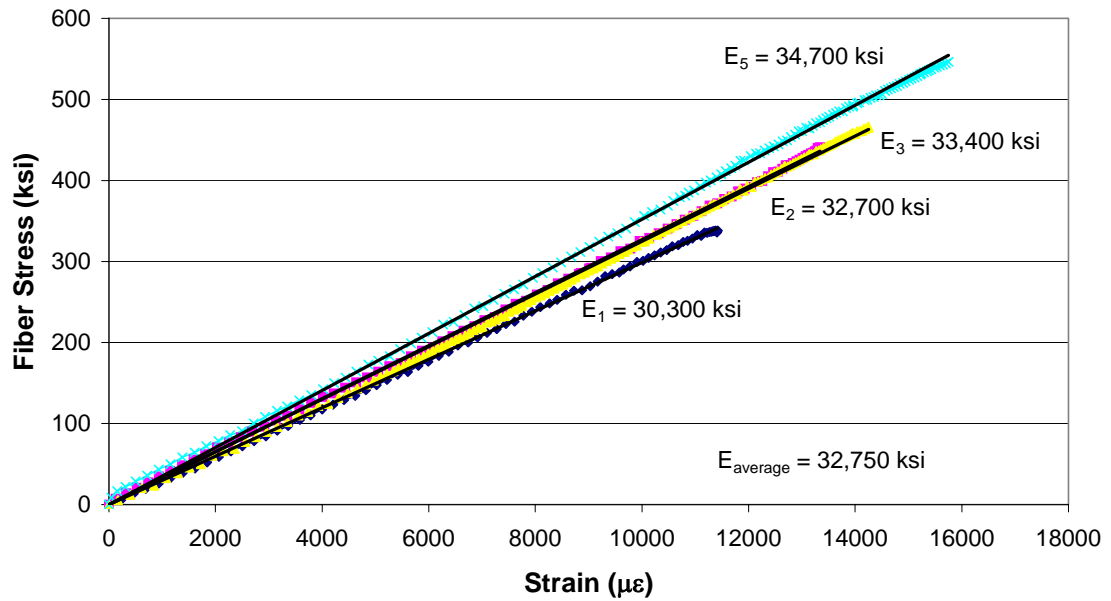
FY-4

Specimen	E_{comp}	E_{fiber}	f_u (fiber)	Failure Mode
1	11,938	21,373	153	AWT
2	6,336	12,467	122	AGT
3	8,978	15,350	132	SGM
4	4,893	8,997	125	SGM
5	5,205	9,570	117	SGM
Average	**7,470**	**13,551**	**130**	
Std Dev	**2,970**	**5,054**	**14**	

Longitudinal Fiber Stress vs. Strain for FY-4 Samples
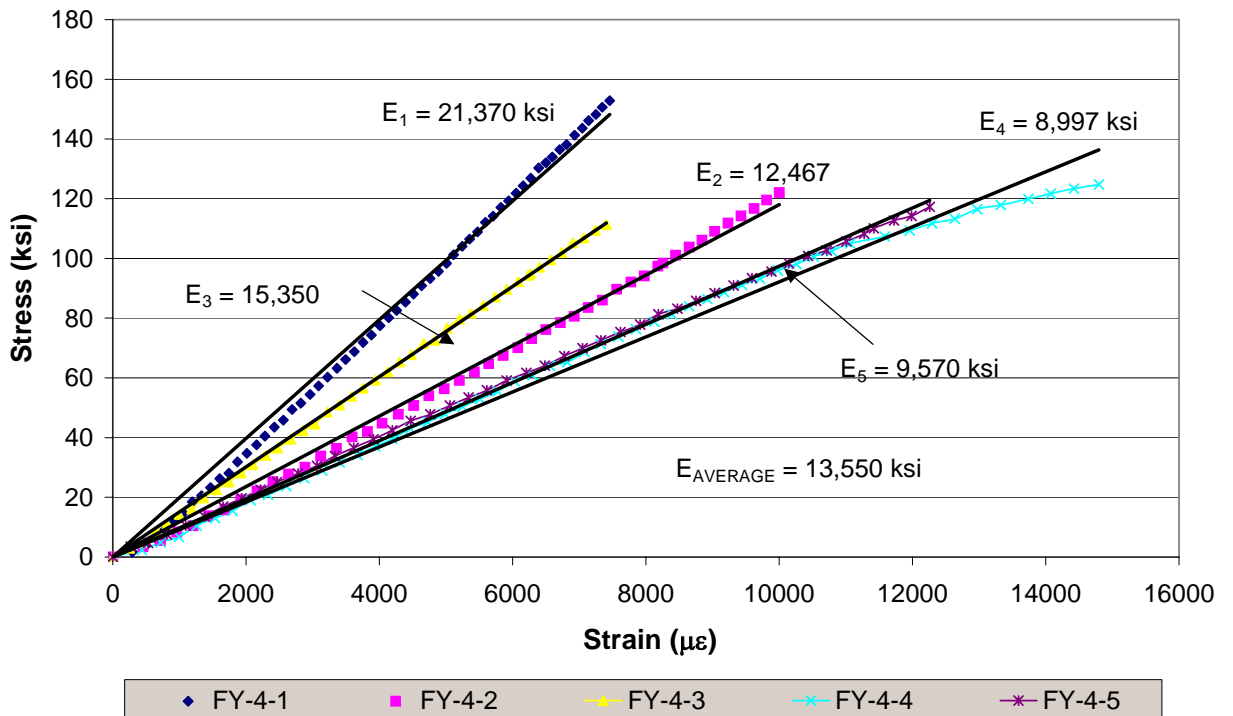
FY-6

Specimen	E_{comp}	E_{fiber}	f_u (fiber)	Failure Mode
1	5,287	13,559	140	LGT
2	4,949	14,289	160	LGT
3 *	8,811	24,160	137	LMM
4	5,262	15,106	180	LGT
5	4,616	13,698	106	LGM
Average	**5,029**	**14,163**	**145**	
Std Dev	**315**	**704**	**28**	

Longitudinal Fiber Stress vs. Strain for FY-6 Samples